J. Fluid Mech. (1991), *vol.* 230, *pp.* 117–146
Printed in Great Britain

Long-wave instabilities of heated falling films: two-dimensional theory of uniform layers

By S. W. JOO[1], S. H. DAVIS[1] AND S. G. BANKOFF[2]

[1] Department of Engineering Sciences and Applied Mathematics, Northwestern University, Evanston, IL 60208, USA

[2] Department of Chemical Engineering, Northwestern University, Evanston, IL 60208, USA

(Received 16 August 1990)

A layer of volatile viscous liquid drains down a uniformly heated inclined plate. Long-wave instabilities of the uniform film are studied by deriving an evolution equation for two-dimensional disturbances. This equation incorporates viscosity, gravity, surface tension, thermocapillarity, and evaporation effects. The linear theory derived from this describes the competition among the instabilities. Numerical solution of the evolution equation describes the finite-amplitude behaviour that determines the propensity for dryout of the film. Among the phenomena that appear are the tendency to wave breaking, the creation of secondary structures, and the pre-emption of dryout by mean flow.

1. Introduction

A liquid layer flowing down an inclined plane is susceptible to long surface-wave instabilities. If the plate is heated, thermocapillary and/or evaporative instabilities may occur, resulting in the dryout of portions of the layer. The present work is devoted to determining the nature of the competitive instabilities, the evolution of the film, and the tendency toward dryout. To this end, a strongly nonlinear evolution equation is derived for two-dimensional disturbances. From this equation the linear stability of the uniform layer is analysed, and the nonlinear evolution of disturbances is examined using numerical simulations.

Yih (1955) and Benjamin (1957) first studied the linear theory for the isothermal falling film. Yih (1963) formulated the problem in terms of long-wave asymptotics and thus determined the critical Reynolds number above which the instability would occur. Benney (1966) extended the theory into the nonlinear regime by deriving a nonlinear evolution equation. There have been a number of extensions of this work as discussed by Atherton & Homsy (1976) and Lin & Wang (1985).

Thermocapillarity has been incorporated into the falling film by Lin (1974), Sreenivasan & Lin (1978), and Kelly, Davis & Goussis (1986). They considered a heated incline and examined the interaction of the two modes of instability, viz. hydrodynamic (or surface-wave) and thermocapillary instability. Kelly *et al.* considered the linear theory, applied the long-wave approximation with arbitrary angle of inclination, and showed that thermocapillarity causes complete destabilization of the film for angles of inclination well below 90°. They also noticed the existence of a stability window; the stable uniform layer can be destabilized by either raising or lowering the Reynolds number. In the present study it will be shown that this phenomenon is caused by the stabilizing effect of hydrostatic pressure, and that an analogous phenomenon can occur for evaporative instability as well.

When the liquid is volatile, another mode of instability is present owing to vapour recoil. This effect was studied by Bankoff (1971), Spindler, Solesio & Delhaye (1978), Spindler (1982), and many others, including most recently Burelbach, Bankoff & Davis (1988), who considered an evaporating layer with heat transfer, but without gravitational effects. They derived the *one-sided model* of evaporation, where the dynamics of the vapour are decoupled from those of the liquid. Using long-wave theory, they obtained an evolution equation for the static layer, which describes the effects of mass loss (or gain for condensing film), surface tension, van der Waals attractions, vapour recoil, and thermocapillarity. They then focused on the development of dryout, and studied the interaction of the effect of various instabilities on the film rupture.

The present study extends the work of Burelbach *et al.* (1988) to include the effects of gravity-driven flow and hydrostatic pressure. In many practical situations, the plate is not horizontal. The flow is driven along the plate by the tangential component of gravity, which in turn changes the heat transfer, and thus the rupture instabilities. When a layer flows downwards, it is subject to surface-wave instability, which can cause steepening and overturning of the liquid–gas interface. Thermocapillary instability acts strongly on surface depressions and draws them toward the heated plate. As the local thickness of the layer decreases, evaporation becomes important, and evaporative instability (owing to vapour recoil) causes the wave trough to thin, after which long-range molecular forces (van der Waals attractions) may take over, and cause the rupture almost instantaneously. Save for the last stage, this sequence of events will be studied herein.

In §2, the flow configuration is explained and the governing system of equations are obtained. In §3, we apply the long-wave approximation and derive an evolution equation for the layer thickness. The equation contains all the hydrodynamic, thermocapillary, and evaporative effects mentioned above. Van der Waals attractions are not considered here. In §4, two basic states are discussed. One is spatially uniform and time-dependent. The other is steady and develops in space. A linear stability analysis for the time-dependent, spatially uniform, basic state is performed in §5, and the nonlinear evolution of various instabilities is examined in §6 using a pseudo-spectral method. We conclude in §7 by summarizing the results.

2. Formulation

We consider a two-dimensional Newtonian liquid of constant density ρ, viscosity μ, and thermal conductivity k, driven by gravity down an inclined plate of angle β to the horizontal, as shown in figure 1. The liquid layer of mean thickness d_0 is bounded above by a free surface and is laterally unbounded. The plate has a fixed constant temperature T_H, and the temperature T_F of the liquid on the free surface is controlled by losses to the passive gas above. The liquid is volatile, and thus the liquid particles change phase to vapour at the free surface. The surface tension σ depends on temperature, so that thermocapillary effects are present.

We use a non-dimensional Cartesian coordinate system (x, z) with origin on the plate, x directed down the incline, and z normal to the plate increasing into the liquid; the coordinates are scaled by d_0. Then, if we use a viscous timescale d_0^2/ν, where $\nu = \mu/\rho$, the Navier–Stokes equations can be written as

$$u_t + uu_x + wu_z = -p_x + u_{xx} + u_{zz} + G\sin\beta, \tag{2.1}$$

$$w_t + uw_x + ww_z = -p_z + w_{xx} + w_{zz} - G\cos\beta, \tag{2.2}$$

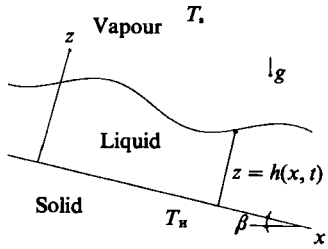

FIGURE 1. The physical configuration of a thin layer flowing down a heated inclined plane.

where u and w are the equation components in the x- and z-directions, respectively, and p is the pressure. Here, $G\sin\beta$ is the Reynolds number, where G is defined as

$$G = \frac{d_0^3 g}{\nu^2}, \tag{2.3}$$

g is the gravitational acceleration, and $\frac{1}{3}gd_0^2\sin\beta/\nu$ is the average velocity of the falling film. The continuity equation is

$$u_x + w_z = 0, \tag{2.4}$$

and the energy equation is

$$P(T_t + uT_x + wT_z) = T_{xx} + T_{zz}. \tag{2.5}$$

Here, P is the Prandtl number

$$P = \nu/\kappa, \tag{2.6}$$

where κ is the thermal diffusivity. The non-dimensional temperature T is defined as

$$T = \frac{T^{\mathrm{D}} - T_{\mathrm{S}}}{T_{\mathrm{H}} - T_{\mathrm{S}}},$$

where T^{D} is the dimensional temperature and T_{S} is the saturation temperature.

The surface tension is assumed to decrease linearly with the temperature:

$$\sigma = \sigma_0 - \gamma(T_{\mathrm{F}} - T_{\mathrm{S}}), \tag{2.7}$$

where σ_0 is the mean surface tension at the saturation temperature and $\gamma\,(= -\mathrm{d}\sigma/\mathrm{d}T)$ is positive for most common liquids.

For evaporation, we adopt the one-sided model of Burelbach *et al.* (1988), which assumes that the density, viscosity, and thermal conductivity of the vapour layer above the free surface are negligible compared to those of the liquid layer, except when multiplied by the (large) vapour velocity. It also uses a linearized version of the constitutive equation of Palmer (1976) to relate the mass flux from the free surface to the local temperature T_{F}. For a detailed derivation of the model and references the reader should refer to Burelbach *et al.* (1988).

With the evaporation model introduced, the normal-stress condition on the free surface at $z = h$ is

$$-\tfrac{3}{2}E^2 J^2/D + p - 2\,[u_x(h_x^2 - 1) - h_x(u_z + w_x)]/N^2 = -3S\,(1 - CT)\,h_{xx}/N^3, \tag{2.8}$$

where $h(x,t)$ is the local thickness of the layer and $N=(1+h_x^2)^{\frac{1}{2}}$. The evaporation number

$$E=\frac{k\Delta T}{\rho\nu L^{\mathrm{D}}}, \tag{2.9}$$

where $\Delta T=T_{\mathrm{H}}-T_{\mathrm{S}}$ and L^{D} is the latent heat, measures the rate of evaporation. The parameter D relates the vapour density ρ^{V} to the liquid density,

$$D=\tfrac{3}{2}\rho^{\mathrm{V}}/\rho, \tag{2.10}$$

and is usually very small. The non-dimensional mass flux $J(x,t)$ is scaled by its value $k\Delta T/d_0L^{\mathrm{D}}$ for a constant flat film. The non-dimensional mean surface tension is

$$S=\frac{\sigma_0 d_0}{3\rho\nu^2}, \tag{2.11}$$

and the capillary number is

$$C=\frac{\gamma\Delta T}{\sigma_0}. \tag{2.12}$$

The terms in (2.8) represent, respectively, the vapour recoil, the pressure, viscous normal-stress jump, and the capillary pressure, which incorporates the temperature-dependent surface tension.

The shear-stress condition on the free surface is unaffected by evaporation, and is given by

$$(u_z+w_x)(1-h_x^2)-4u_xh_x=-2NM(T_x+h_xT_z)/P, \tag{2.13}$$

where M is the Marangoni number,

$$M=\frac{\gamma\Delta Td_0}{2\mu k}. \tag{2.14}$$

The energy balance on the free surface gives

$$J+\frac{E^2}{D^2L}J^3=\frac{h_xT_x-T_z}{N}, \tag{2.15}$$

where L is the non-dimensional latent heat defined as

$$L=\frac{8d_0^2L^{\mathrm{D}}}{9\nu^2}. \tag{2.16}$$

As described by Burelbach *et al.* (1988), the energy-balance condition (2.15) states that the heat conducted across the surface is used to vaporize the liquid particles and impart kinetic energy to the vapour particles.

The linear constitutive relationship on the free surface is written as

$$KJ=T. \tag{2.17}$$

The parameter K is defined as

$$K=\frac{kT_{\mathrm{S}}^{\frac{3}{2}}}{\alpha d_0\rho^{\mathrm{V}}(L^{\mathrm{D}})^2}\left(\frac{2\pi R_{\mathrm{g}}}{M_{\mathrm{W}}}\right)^{\frac{1}{2}}, \tag{2.18}$$

where R_{g}, M_{W}, and α, respectively, are the universal gas constant, the molecular weight, and the accommodation constant (see Palmer 1976). It measures the degree of non-equilibrium on the free surface. $K=0$ represents the case of a constant free-surface temperature, $T_{\mathrm{F}}=T_{\mathrm{S}}$, while $K\to\infty$ gives the zero-evaporation limit, $J=0$.

The last boundary condition on the free surface is the kinematic condition. Since the particles on the free surface are evaporating, the kinematic condition for a material surface is modified by mass loss:

$$EJ = \frac{w - h_t - uh_x}{N}. \tag{2.19}$$

If one sets $J = 0$, one obtains the kinematic boundary condition for a material surface.

On the heated plate, we assume no penetration and no slip and impose a constant-temperature condition. Therefore, the boundary condition at $z = 0$ are

$$u = w = T = 0. \tag{2.20}$$

3. Long-wave theory

In many practical situations, interfacial instabilities are locally generated and hence do not scale on layer thicknesses; the waves are long (see Lin & Wang 1985). Therefore, we focus our interest on flows with a characteristic length in the x-direction, l_c, much larger than the thickness of the layer, where l_c typically is proportional to the disturbance wavelength. We then follow Benney's (1966) expansion for the small wavenumber $\epsilon = d_0/l_c$.

We rescale the system (2.1)–(2.20) using a lubrication-type approximation by introducing

$$\xi = \epsilon x, \quad \zeta = z, \quad \tau = \epsilon t. \tag{3.1}$$

For an isothermal falling film it is well known that the terms that cause the surface-wave instability appear in the second approximation when the Reynolds number is $O(1)$ (see e.g. Atherton & Homsy 1976). In the present study we scale the parameters such that the thermal instabilities also appear at the second order and these compete with each other. While the other parameters remain $O(1)$, we set

$$(E, D, S) = (\epsilon\bar{E}, \epsilon^2\bar{D}, \epsilon^{-2}\bar{S}), \tag{3.2}$$

where the barred quantities are $O(1)$. Burelbach *et al.* (1988) tabulated numerical values of these parameters for thin layers of water and of ethanol, which suggest that the scales taken in (3.2) can be realistic. The scales (3.2) make both E^2/D (vapour recoil) and KM/P (thermocapillarity) of $O(1)$ and thus they appear in the evolution equation at the second order.

The dependent variables are expanded for small ϵ;

$$u = u_0 + \epsilon u_1 + \ldots, \tag{3.3}$$

$$w = \epsilon(w_0 + \epsilon w_1 + \ldots), \tag{3.4}$$

$$p = p_0 + \epsilon p_1 + \ldots, \tag{3.5}$$

$$T = T_0 + \epsilon T_1 + \ldots, \tag{3.6}$$

$$J = J_0 + \epsilon J_1 + \ldots, \tag{3.7}$$

where $h = O(1)$.

We then substitute the expansions (3.3)–(3.7) into the rescaled governing equations and obtain the solutions for the dependent variables. We display some of the results for future reference. The velocity component in the x-direction is

$$u(\xi, \zeta, \tau) = G(h\zeta - \tfrac{1}{2}\zeta^2)\sin\beta + \epsilon\Big\{(Gh_\xi\cos\beta - \Phi)(\tfrac{1}{2}\zeta^2 - h\zeta) + \tfrac{1}{2}Gh_\tau(\tfrac{1}{3}\zeta^3 - h^2\zeta)\sin\beta$$
$$+ \tfrac{1}{6}G^2 hh_\xi(\tfrac{1}{4}\zeta^4 - h^3\zeta)\sin^2\beta + 2\frac{M}{P}\left(\frac{h}{h+K}\right)_\xi \zeta\Big\} + O(\epsilon^2), \tag{3.8}$$

where $$\Phi = 3\frac{E^2}{D}\frac{h_\xi}{(h+K)^2} + 3\bar{S}h_{\xi\xi\xi}.$$

It shows that the local volumetric flow rate accurate up to the second-order depends on h and its derivatives in addition to the parameters. The velocity component in the z-direction, evaluated on the free surface, is

$$\begin{aligned} w(\xi,h,\tau) = -\epsilon\tfrac{1}{2}Gh^2h_\xi\sin\beta + \epsilon^2\Big\{ & Gh^2(\tfrac{1}{3}hh_{\xi\xi}+\tfrac{1}{2}h_\xi^2)\cos\beta - h^2(\tfrac{1}{3}h\Phi_\xi+\tfrac{1}{2}h_\xi\Phi) \\ & + Gh^3(\tfrac{5}{24}hh_{\tau\xi}+\tfrac{1}{2}h_\xi h_\tau)\sin\beta + \tfrac{1}{40}G^2h^5(13h_\xi^2+3hh_\xi)\sin^2\beta \\ & - \frac{M}{P}h^2\left(\frac{h}{h+K}\right)_{\xi\xi}\Big\} + O(\epsilon^3). \end{aligned} \tag{3.9}$$

The leading-order pressure,

$$p_0 = G(h-\zeta)\cos\beta + \frac{3}{2}\frac{E^2}{D}\frac{1}{(h+K)^2} - 3\bar{S}h_{\xi\xi}, \tag{3.10}$$

is composed of hydrostatic pressure, vapour recoil, and capillary effects. The temperature field and the evaporative mass flux are, respectively,

$$T = 1 - \frac{\zeta}{h+K} + O(\epsilon) \tag{3.11}$$

and $$J = \frac{1}{h+K} - \epsilon P\left(\frac{h}{h+K}\right)^3[\tfrac{1}{3}h_\tau + \tfrac{1}{40}G(11h+5K)\,hh_\xi\sin\beta] + O(\epsilon^2). \tag{3.12}$$

The heat transfer is purely conductive to the leading order, but is modified by second-order unsteady and convective effects.

The above solutions are substituted into the kinematic condition (2.19), resulting in an evolution equation for the film thickness h:

$$\begin{aligned} & h_\tau + \frac{\bar{E}}{h+K} + Gh^2h_\xi\sin\beta \\ & \quad + \epsilon\left[\frac{2G^2}{15}h^6h_\xi\sin^2\beta + \frac{KM}{P}\frac{h^2h_\xi}{(h+K)^2} + \frac{E^2}{D}\frac{h^3h_\xi}{(h+K)^3} - \tfrac{1}{3}Gh^3h_\xi\cos\beta + \bar{S}h^3h_{\xi\xi\xi}\right]_\xi \\ & + \epsilon\bar{E}\frac{5G}{24}\left(\frac{h^4}{h+K}\right)_\xi\sin\beta + \epsilon\bar{E}P\left(\frac{h}{h+K}\right)^3\left[\frac{\bar{E}}{3(h+K)} + \frac{G}{120}(7h-15K)\,hh_\xi\sin\beta\right] = 0. \end{aligned} \tag{3.13}$$

The terms proportional to $\bar{E}$ in (3.13) describe the mass loss due to evaporation, while the third term describes wave propagation and steepening. The fourth, fifth, and sixth terms describe mean shear flow, thermocapillarity, and vapour recoil, respectively, and generate instabilities as shown below. The next two terms represent hydrostatic effects and mean surface tension.

In the isothermal limit ($\bar{E}, E^2/D, KM/P \to 0$), equation (3.13) reduces to the evolution equation for falling films obtained by Benney (1966), Krantz & Goren (1971), and Atherton & Homsy (1976). When G is negative and $\beta = 0$, it describes Rayleigh–Taylor instability in thin viscous films with small Bond number (Yiantsios & Higgins 1989). In the zero-gravity limit ($G \to 0$), equation (3.13) generalizes the equation of Burelbach *et al.* (1988) for a static evaporating film to unit-order M and P. This then includes $O(\epsilon)$ effects of convection and evaporation.

When $\bar{E} = 0$ and $E^2/D = 0$, the equation (3.13) describes the evolution of a non-volatile layer with thermocapillarity and gravity. In this case, the mass flux $J = 0$, and the boundary conditions (2.15) and (2.17) can be combined to give a condition for the temperature field on the free surface. The reference temperature T_S then can be considered as an ambient temperature. Up to the order taken in (3.13), the resulting thermal boundary condition is $T + KT_z = 0$ at the free surface, so that the parameter K^{-1} is the Biot number and is no longer defined by (2.18). Instead, it represents a dimensionless heat transfer coefficient. In the small-Biot-number limit ($K^{-1} \to 0$), the thermocapillary term in (3.13) can be simplified as $\mathcal{M}h^2h_\xi$, where $\mathcal{M}$ ($= MK^{-1}P^{-1}$) is the effective Marangoni number. Then, if we further set $\beta = 0$, the evolution equation (3.13) reduces to that obtained by Davis (1983) when van der Waals effects, retained by him, are neglected.

4. Basic states

Two sets of solutions to the governing system in §2 are of particular interest. One is spatially uniform and time-dependent. It describes an infinitely long flat layer that drains downward and disappears in a finite time. The second basic state is steady and develops in space. It describes a steady layer, which thins in the flow direction and terminates at a contact line.

When a flat layer is placed on a plate and tilted, it flows downward along the plate. At the same time it thins owing to evaporation if the plate is heated and the liquid is volatile. The corresponding flow and temperature field can be obtained by solving the governing system in §2 with $\partial_x = 0$. The velocity component in the x-direction has a parabolic profile and that in the z-direction is zero. The temperature is unity on the heated plate and decreases to

$$\frac{K}{h+K}\left[1+\tfrac{1}{3}\epsilon\bar{E}P\left(\frac{h}{h+K}\right)^3\right]$$

on the free surface. The layer thickness is independent of x, and can be obtained by solving the evolution equation (3.13) with $\partial_\xi = 0$:

$$h_0 = \Omega - K + \epsilon\frac{\bar{E}P}{3\Omega}\left(\frac{K(2K^2+6K+3)}{1+K}+\frac{3K^2}{2}\ln\frac{\Omega}{1+K}+\frac{K^3}{\Omega}-3K\Omega-\bar{E}\tau\right)+O(\epsilon^2), \quad (4.1)$$

where $\Omega(\tau) = ((1+K)^2 - 2\bar{E}\tau)^{\frac{1}{2}}$ and h_0 indicates a basic state. The free-surface configuration (4.1) does not depend on Reynolds number, and generalizes the state considered by Burelbach *et al.* (1988) for static evaporating layers to second order. The layer thins uniformly and disappears at a finite time. When $P = 0$, the disappearance time is $\tau = (1+2K)/(2\bar{E})$, and it decreases with P. When mass loss is absent ($\bar{E} = 0$), equation (4.1) reduces to $h_0 = 1$, which is considered by Yih (1963), among others, for isothermal conditions and Kelly *et al.* (1986) for layers with thermocapillarity.

The second basic state can be reached by feeding the flow at the upstream end at a given flow rate. The fluid then flows downstream with the total evaporative mass flux across the interface balancing the flow fed upstream. The free-surface configuration for this steady basic state can be obtained by solving the evolution equation (3.13) with $\partial_\tau = 0$ in a finite domain $0 \leqslant \xi \leqslant a$. Here, $\xi = 0$ is a fixed point on the incline (e.g. an exit of reservoir through which the fluid is fed), and $\xi = a$ is the *a priori* unknown location of the contact line.

Both of these states are important to consider. In the present study, we consider only the spatially uniform basic state, and study its stability to long-wave disturbances.

5. Linear stability analysis

We first apply a linear stability analysis, consider a simple harmonic disturbance of small amplitude to state (4.1), and write the solution of equation (3.13) as follows:

$$h = h_0(\tau) + \delta[H(\tau)\,\mathrm{e}^{\mathrm{i}k\xi} + \text{c.c.}]. \tag{5.1}$$

Here δ is the initial amplitude of the disturbance, H is the time-dependent normal-mode amplitude having $H(0) = \frac{1}{2}$, k is the scaled disturbance wavenumber, and c.c. denotes the complex conjugate. We substitute the above expression into (3.13) and linearize in δ to obtain

$$\dot{H}/H = \Gamma_{\mathrm{ev}}(\tau) + \Gamma(\tau) - \mathrm{i}kc(\tau), \tag{5.2}$$

where

$$\Gamma = \epsilon k^2\left[\frac{E^2}{D}\left(\frac{h_0}{h_0+K}\right)^3 + \frac{KM}{P}\left(\frac{h_0}{h_0+K}\right)^2 + \frac{2G^2}{15}h_0^6\sin^2\beta - \frac{G}{3}h_0^3\cos\beta - k^2\bar{S}h_0^3\right] \tag{5.3}$$

is defined as an effective growth rate,

$$c = G\left[1 + \epsilon\frac{5\bar{E}}{24}\left\{\frac{4h_0}{h_0+K} - \left(\frac{h_0}{h_0+K}\right)^2 + \frac{Ph_0^2(7h_0-15K)}{25(h_0+K)^3}\right\}\right]h_0^2\sin\beta \tag{5.4}$$

is the linearized phase speed, and

$$\Gamma_{\mathrm{ev}} = \frac{\bar{E}}{(h_0+K)^2} + \epsilon\bar{E}P\frac{h_0^2(h_0-3K)}{3(h_0+K)^5}. \tag{5.5}$$

The term Γ_{ev} is real, but does not affect the effective growth. It measures the initial disturbance amplitude relative to the decaying thickness of the basic state, and involves no instability. Upon integration of (5.2), it gives an algebraic variation† in H. The phase speed c decreases with time as the layer thins, and so indicates that the wave propagation can be affected by evaporation.

The effective growth rate $\Gamma(\tau)$ shows the destabilizing effects of vapour recoil, thermocapillarity, and mean flow and the stabilizing effects of hydrostatic pressure and surface tension. In the presence of surface tension ($\bar{S} \neq 0$), there is a cutoff wavenumber k_c above which no instability is present; k_c is obtained by setting $\Gamma = 0$ and depends parametrically on time. The maximum growth rate occurs at $k = k_c/\sqrt{2}$. In the absence of mass loss ($\bar{E} = 0$), the basic state has $h_0 \equiv 1$, and the condition for instability is $\Gamma > 0$. When heat transfer and surface tension are neglected, it yields the instability condition

$$G\sin\beta > \tfrac{5}{2}\cot\beta, \tag{5.6}$$

obtained by Benjamin (1957) and Yih (1963).

Figure 2 shows the effects of gravity, vapour recoil, and thermocapillarity on the stability of film flow when $\bar{S} = 0$. The growth rate Γ is negative *inside* the space Σ_S bounded by the $(G, E^2/D)$- and $(G, KM/P)$-planes and the neutral surface. Projection

† A referee suggested an alternative to the removal of Γ_{ev} after the integration. For $P = 0$, say, if we define $y = \frac{1}{2}(h+K)^2$ and write $y = y_0 + \delta[Y(\tau)\,\mathrm{e}^{\mathrm{i}k\xi} + \text{c.c.}]$ in place of (5.1), then $\partial y_0/\partial\tau = -\bar{E}$. This procedure removes Γ_{ev} in (5.2).

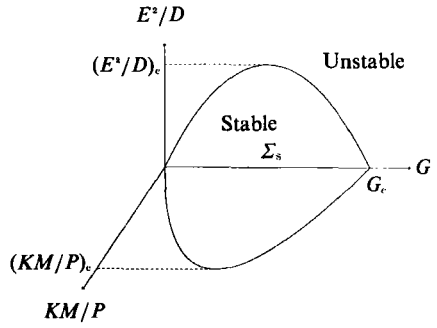

FIGURE 2. Stability diagram of a thin layer when $\bar{S} = 0$.

of the neutral surface onto the $(E^2/D, KM/P)$-plane yields straight lines of equal slope; projection onto the $(G, E^2/D)$- and $(G, KM/P)$-planes yields parabolas of equal curvature. The critical Reynolds number is given by

$$G_c \sin\beta = \frac{5}{2}\frac{\cot\beta}{h_0^3}, \tag{5.7}$$

and the critical values for E^2/D and KM/P are given by

$$\left(\frac{E^2}{D}\right)_c = \frac{5}{12}\left(\frac{h_0+K}{h_0}\right)^3 \cot^2\beta \tag{5.8}$$

and

$$\left(\frac{KM}{P}\right)_c = \frac{5}{24}\left(\frac{h_0+K}{h_0}\right)^2 \cot^2\beta. \tag{5.9}$$

When we set $E^2/D = KM/P = 0$ and move along the G-axis, the segment outside of Σ_S corresponds to surface-wave instability (see (5.6)). When we set $0 < E^2/D < (E^2/D)_c$ with $KM/P = 0$, and move along a straight line parallel to the G-axis, there is a positive growth rate for small G, owing to evaporative instability, and then a negative value, owing to the stabilizing effect of hydrostatic pressure. However, at large enough G there is again growth, because of surface-wave instability. This same sequence of instability, stability, and then instability as G increases has been predicted by Kelly *et al.* (1986) for the case with only thermocapillary effects. As can be seen from (5.7)–(5.9), the space Σ_S expands with time as the layer gets thinner and thinner. Of the three critical values, G_c increases most rapidly, while $(KM/P)_c$ changes slowest. Intuitively, this is obvious, because the thinner the layer the more viscous resistance there is to fluid flow.

When surface tension is present, the stable region Σ_S increases in size as shown in figure 3. When $G = 0$, both E^2/D and KM/P acquire upper bounds for instability; the destabilizing effects of vapour recoil and thermocapillarity are now effective only for disturbances with sufficiently small wave number. The critical Reynolds number is also increased to

$$G_c \sin\beta = \frac{1}{2h_0^3}\{\tfrac{5}{2}\cot\beta + [(\tfrac{5}{2}\cot\beta)^2 + 30k^2\bar{S}h_0^3]^{\frac{1}{2}}\}. \tag{5.10}$$

As the layer thins, the intersection between the neutral surface and the $(E^2/D, KM/P)$-plane approaches the origin, so that surface tension becomes less effective.

There are two distinct limits, in which the thermocapillary instability disappears. As mentioned above, the parameter K^{-1} can be interpreted as the Biot number for

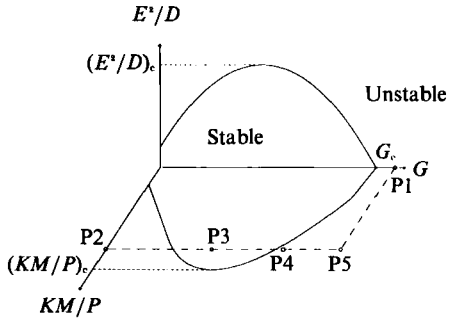

FIGURE 3. Stability diagram of a thin layer.

non-volatile layers. The contribution of the thermocapillarity to the effective growth rate Γ vanishes for either $K^{-1} \to 0$ or $K^{-1} \to \infty$. When the heat transfer coefficient is small ($K^{-1} \to 0$), the free surface behaves as a fixed-flux boundary ($T_z = 0$ at $z = h$). The vertical temperature gradient in the layer then disappears, and the temperature is everywhere identical to that of the bottom plate. When the heat transfer coefficient is large ($K^{-1} \to \infty$), the free surface is a perfect conductor ($T = 0$ at $z = h$). The temperature along the surface is then the constant ambient temperature.

6. Nonlinear evolution of the infinite layer

The linear analysis in §5 is valid as long as disturbance amplitudes stay small. In order to examine the nonlinear evolution of instabilities, we must solve (3.13). We pose an initial-value problem on a periodic domain and solve it using a Fourier-spectral method.

The initial condition is taken to be a simple-harmonic disturbance superimposed on the flat interface,

$$h(\xi, 0) = 1 - \delta \cos(k\xi), \tag{6.1}$$

where $\delta = 0.1$. The solution is approximated by a finite Fourier series

$$h(\xi, \tau) = \sum_{n=-N}^{N} a_n e^{ikn\xi} + \text{c.c.} \quad \left(-\frac{\pi}{k} \leqslant \xi \leqslant \frac{\pi}{k}\right) \tag{6.2}$$

with $N \geqslant 64$. The computational domain is set to be the interval $[0, 2\pi/k]$. In the cases shown below, we take $\epsilon = 0.2$ and $\bar{S} = 0.1$. The time marching is done by a fourth-order Hamming modified predictor–corrector method with a maximum error bound of 10^{-11}. The fourth-order Runge–Kutta method is used for automatic adjustment of the initial increment and for the computation of starting values. At each time step, the spectral coefficients are checked in order to monitor the spatial resolution. Aliasing errors are suppressed by taking a large number of collocation points and discarding the higher half of the Fourier modes. For evaporating layers, we stop the numerical integration as soon as the local minimum layer thickness becomes smaller than the maximum error bound 10^{-11}, and define the corresponding time as the rupture time τ_R.

6.1. *Isothermal layers* ($G, \bar{S} \neq 0; \bar{E} = E^2/D = KM/P = 0$)

We examine the evolution of surface waves on isothermal layers. The nonlinear evolution of isothermal layers has been studied analytically by Gjevik (1970), Lin (1974), Tougou (1981), and Chang (1989) among others. Gjevik (1970) and Tougou

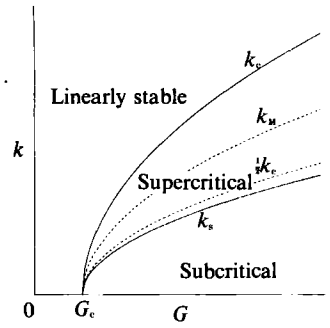

FIGURE 4. Stability diagram of isothermal layers.

(1981) considered waves with initial wavenumbers close to the cutoff wavenumber $k = k_c$, and analysed subsequent evolutions by examining the fundamental mode and its lowest harmonics. (This is equivalent to setting $N = 2$ in (6.2).) Lin (1974) performed a weakly nonlinear analysis near the critical Reynolds number $G\sin\beta = G_c\sin\beta$, and transformed the evolution equation (3.13) into a Landau–Stuart equation. He finds that there is a transition point $k = k_s$ that separates supercritical ($k > k_s$) from subcritical ($k < k_s$) bifurcation (see figure 4 and the discussion below). The weakly nonlinear analysis near criticality is generalized by Chang (1989), who obtained various solutions of finite-amplitude permanent waves. Some of the results of these authors relevant to our computations are illustrated in figure 4.

In figure 4, the linear/nonlinear stability diagram is plotted on the (k, G)-plane. The bifurcation point G_c, the upper neutral curve $k = k_c$, the wavenumber $k = k_M$ for maximum liner growth rate, the curve $k = \frac{1}{2}k_c$, and the lower neutral curve $k = 0$ are obtained from the linear theory. The flow is linearly unstable if $G > G_c$ and $0 < k < k_c$. However, when $k > k_s$, capillarity weakens the growth, so that the secondary flow equilibrates; the bifurcating solution is supercritical. If k is sufficiently close to k_c, the harmonics of the fundamental wavenumber are small, and the equilibrated state is a nearly sinusoidal permanent wave, which corresponds to the 'periodic flow' observed by Kapitza & Kapitza (1949). If k is near k_s, a few lowest harmonics are excited due to the nonlinear interaction, and the equilibrated state thus resembles the 'single wave' observed by Kapitza & Kapitza (1949) and studied analytically and numerically by Pumir, Manneville & Pomeau (1983) in terms of solitary waves. When $k < k_s$, the flow is linearly unstable and the nonlinearities augment the growth. Local to the bifurcation point the instability is subcritical. The harmonics excited lie in the linearly unstable regime and grow in a complicated manner owing to their nonlinear interactions. The critical wavenumber k_s gives the transition point that separates the regimes of subcritical and supercritical instability. It coincides with $\frac{1}{2}k_c$ for $\epsilon \to 0$. The $O(\epsilon^2)$ correction on k_s, which depends on G, $\bar{S}$, and β, is exaggerated in figure 4 for clarity. The value k_s increases with G and decreases with $\bar{S}$ and $\frac{1}{2}\pi - \beta$. An asymptotic value of k_s from the weakly nonlinear theory can be obtained from the results of Gjevik (1970), Lin (1974), and Tougou (1981).

We solve the evolution equation (3.13) for isothermal layers with $G = 5$ and $\beta = 45°$, corresponding to point P1 in figure 3. In this case $G_c = 2.5\sqrt{2}$, $k_c \approx 2.21$, and $k_M \approx 1.56$.

Figure 5 shows the surface-wave instability with the initial disturbance wavenumber $k = 2.1$, near the cutoff. In figure 5 (a, b) free-surface shapes are shown with each line representing a time increment of 0.05. For small time, the disturbance

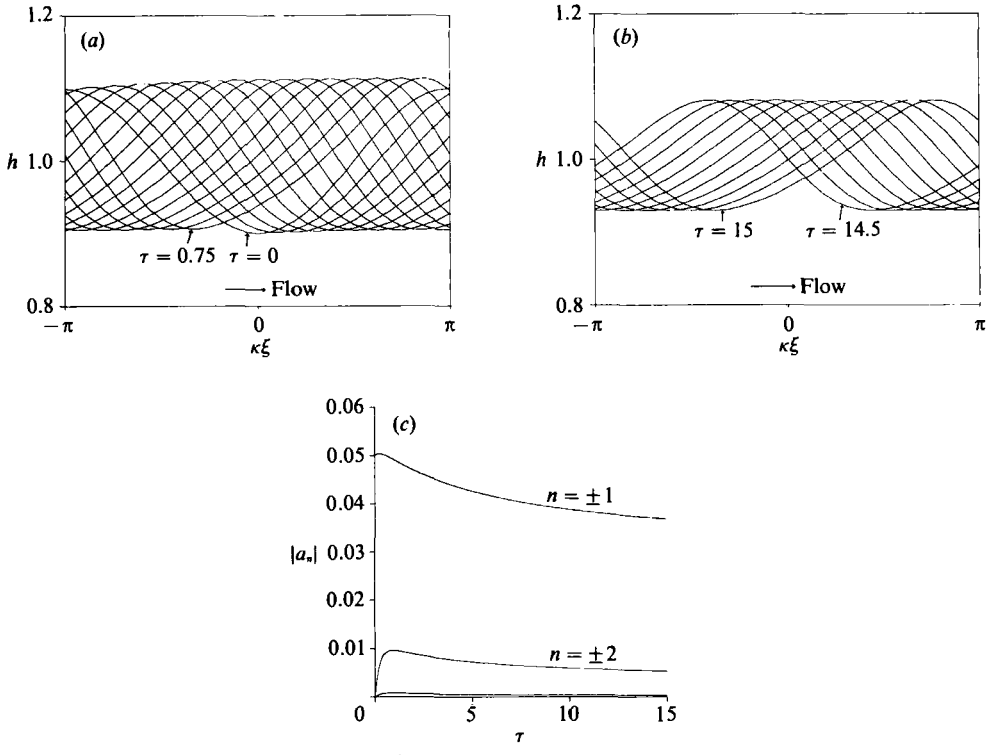

FIGURE 5. Surface-wave instability for an isothermal layer with $k = 2.1$ ($k_M = 1.56$), $G = 5$, $\beta = 45°$, and $\bar{S} = 0.1$: (*a*) free-surface configurations for $0 \leqslant \tau \leqslant 0.75$ with $\Delta\tau = 0.05$; (*b*) free-surface configurations for $14.5 \leqslant \tau \leqslant 15$ with $\Delta\tau = 0.05$; (*c*) evolution of the spectral coefficients.

grows, consistent with the linear theory, but soon reaches a maximum and then decays with the growth of its lowest harmonics ($n = \pm 2$). The harmonics distort the surface slightly from the initial sinusoidal shape, so that the front steepens and the rear is stretched. The harmonics generated have large decay rate according to the linear theory, and so decrease monotonically after the initial generation. The disturbance thus equilibrates, as shown in figure 5(*b*). The magnitudes of the harmonics are small compared to the fundamental, so that the final state is almost sinusoidal as predicted by the weakly nonlinear analysis. In figure 5(*c*) the magnitudes of the fundamental and its first several harmonics are plotted against the time τ. All the modes shown grow initially but soon decay monotonically and converge to constant values. Modes higher than $n = \pm 3$ are very small.

In figure 6, the initial disturbance wavenumber is k_M. Figure 6(*a–c*) shows the evolution of free-surface shapes for initial growth, intermediate decay, and equilibration, respectively. Each line again represents a time increment of 0.05. The initial exponential growth is much more pronounced compared to the previous case, as can also be deduced from the linear theory. The decay rates of the harmonics generated are also smaller than the previous ones, so that the distortion of the surface shape is more significant, as seen in figure 6(*b*). The permanent wave shown in figure 6(*c*) has steeper fronts and longer rears with the presence of the dimples due to harmonics. The magnitude of each spectral coefficient in figure 6(*d*) shows the equilibration of each mode as before, but the limiting values are now larger.

If we take an initial disturbance wavenumber k smaller than k_M but larger than k_s, we may expect more significant contributions of the harmonics. In figure 7, we show

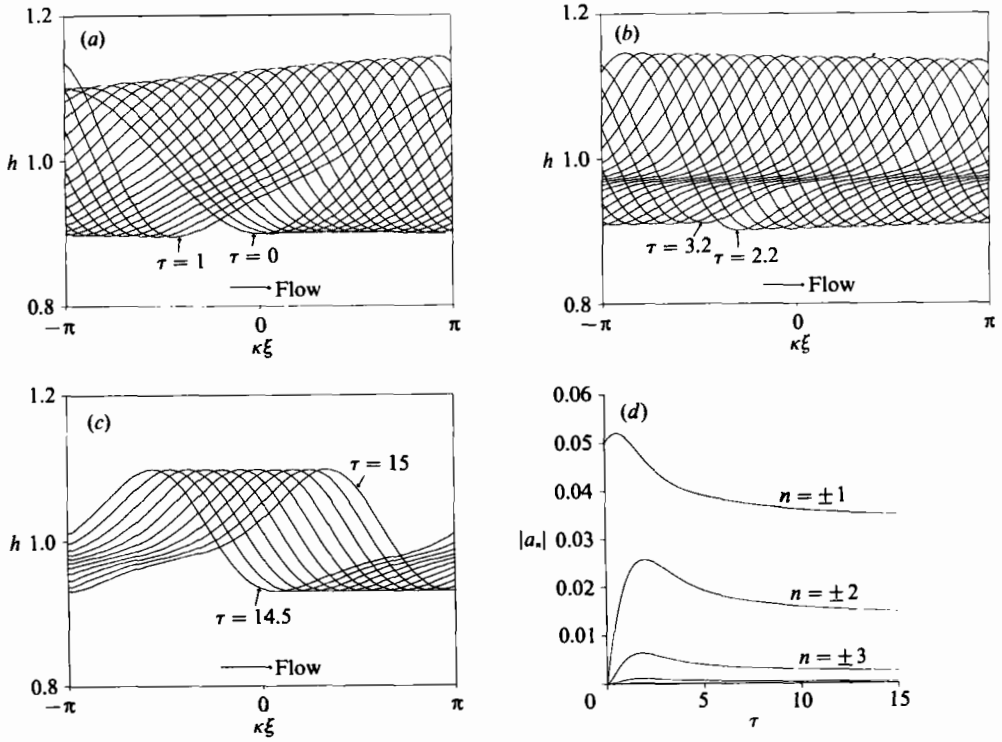

FIGURE 6. Surface-wave instability for an isothermal layer with $k = k_M$, $G = 5$, $\beta = 45°$, and $\bar{S} = 0.1$: (*a*) free-surface configurations for $0 \leqslant \tau \leqslant 1$ with $\Delta\tau = 0.05$; (*b*) free-surface configurations for $2.2 \leqslant \tau \leqslant 3.2$ with $\Delta\tau = 0.05$; (*c*) free-surface configurations for $14.5 \leqslant \tau \leqslant 15$ with $\Delta\tau = 0.05$; (*d*) evolution of the spectral coefficients.

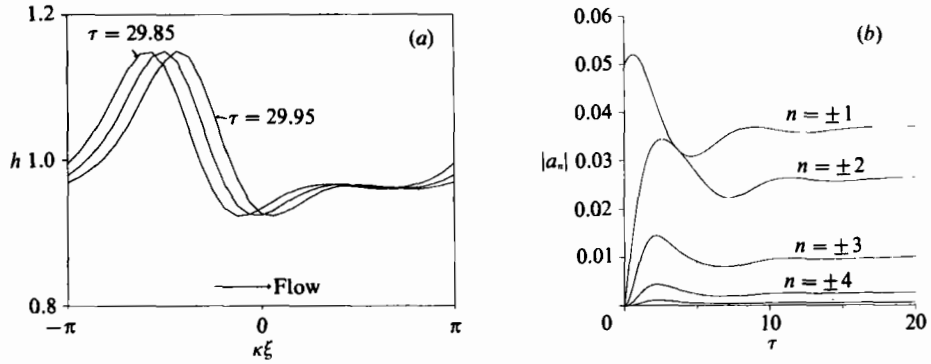

FIGURE 7. Surface-wave instability for an isothermal layer with $k = 1.3$, $G = 5$, $\beta = 45°$, and $\bar{S} = 0.1$: (*a*) free-surface configurations for $29.85 \leqslant \tau \leqslant 29.95$ with $\Delta\tau = 0.05$; (*b*) evolution of the spectral coefficients.

a case with $k = 1.3$. The initial instability and the subsequent decay of the fundamental due to the growth of harmonics are qualitatively the same as in the previous cases. However, the convergence to the equilibrium state is not monotonic. The modes interact with each other and rearrange their magnitudes to form a finite-amplitude permanent wave as shown in figure 7(*b*): this resembles the 'single wave' observed by Kapitza & Kapitza (1949) and computed by Pumir *et al.* (1983). The initial condition used by Pumir *et al.* (1983) is a localized disturbance, which has a

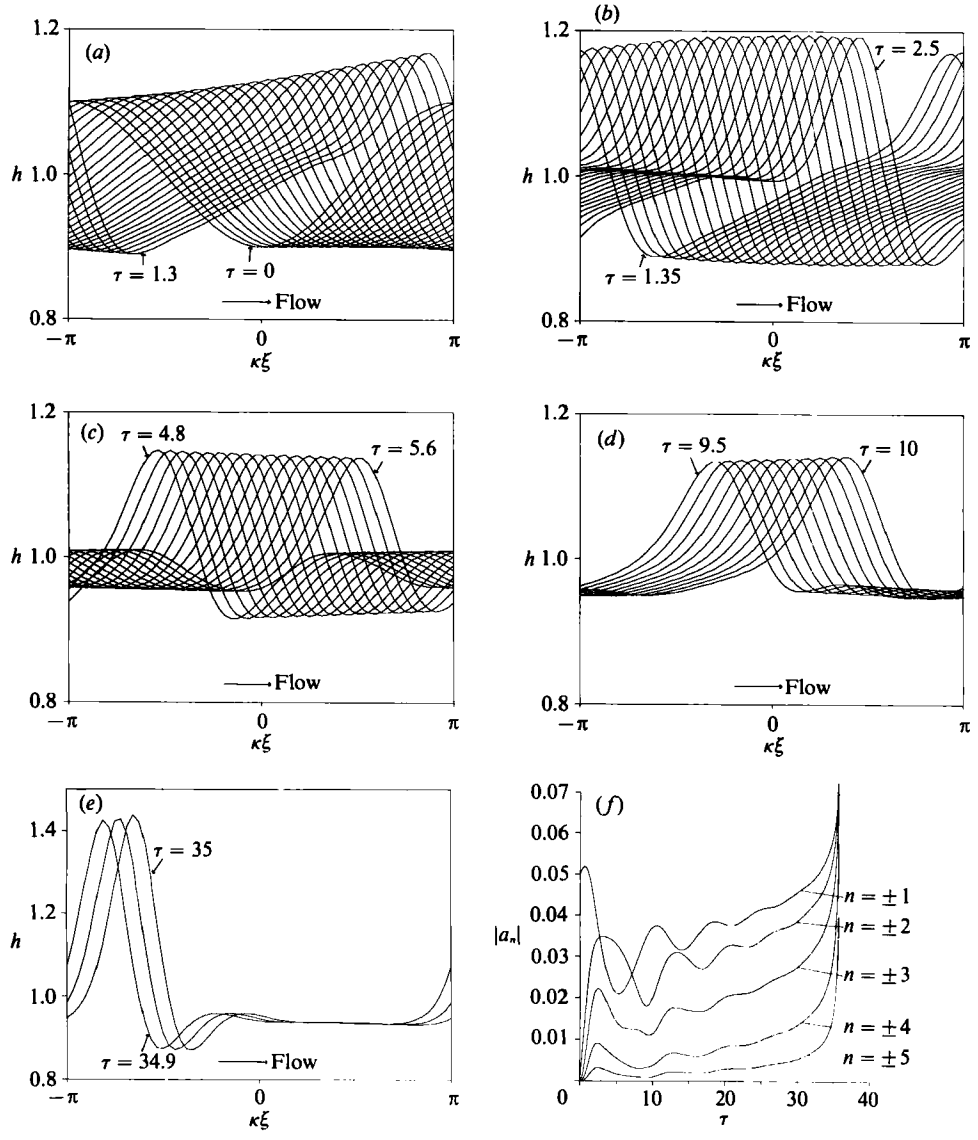

FIGURE 8. Surface-wave instability for an isothermal layer with $k = 1.11$, $G = 5$, $\beta = 45°$, and $\bar{S} = 0.1$: (*a*) free-surface configurations for $0 \leqslant \tau \leqslant 1.3$ with $\Delta\tau = 0.05$; (*b*) free-surface configurations for $1.35 \leqslant \tau \leqslant 2.5$ with $\Delta\tau = 0.05$; (*c*) free-surface configurations for $4.8 \leqslant \tau \leqslant 5.6$ with $\Delta\tau = 0.05$; (*d*) free-surface configurations for $9.5 \leqslant \tau \leqslant 10$ with $\Delta\tau = 0.05$; (*e*) free-surface configurations for $34.9 \leqslant \tau \leqslant 35$ with $\Delta\tau = 0.05$; (*f*) evolution of the spectral coefficients.

continuous spectrum of wavenumbers at $\tau = 0$. Here, we show that even if the initial state is a monochromatic wave, it can evolve into the 'single wave' through nonlinear modal interactions. Kapitza & Kapitza (1949) also observed the 'single wave' by reducing the frequency of the periodic disturbance at the leading edge.

In figure 8, the initial wavenumber $k = 1.11$ is very close to $\frac{1}{2}k_c = 1.105$. According to weakly nonlinear analysis, the flow should equilibrate. However, the computations show no equilibration within the validity of the long-wave approximation, since the higher harmonics are important away from the bifurcation point. Figure 8(*a–e*) shows the free-surface shapes for time increments of 0.05, while figure 8(*f*) shows the

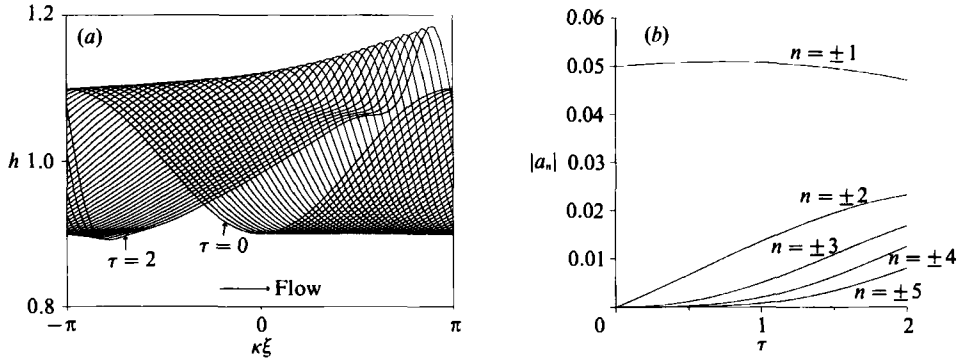

FIGURE 9. Gravitational instability for an isothermal layer with $k = 0.7$, $G = 5$, $\beta = 45°$, and $\bar{S} = 0.1$: (*a*) free-surface configurations with $\Delta\tau = 0.05$ up to $\tau = 2$; (*b*) evolution of the spectral coefficients.

evolution of the first five spectral coefficients. Figure 8(*a*) represents the initial instability. The rapid evolution and growth of the harmonics make the wave fronts steeper and create the dimples at a much earlier stage. The continuously growing harmonics, modes $n = \pm 2$ in particular, receive energy from the fundamental. In figure 8(*b*) and 8(*c*), the initial wave amplitude decays after reaching a maximum, while the dimples grow significantly. In figure 8(*d*) the fundamental recaptures the energy and dominates, while the harmonics decay. Therefore, we observe that the initial crests grow while the dimples decay. This competition between the fundamental and the harmonics continues, so that the initial crests grow and then decay several more times. Eventually still higher harmonics contribute to the evolution, and so the 'single wave' in figure 8(*e*) grows 'explosively'. Clearly, our asymptotic representation breaks down here. For sufficiently large G, similar 'catastrophic' behaviour has been observed by Pumir *et al.* (1983) using a localized initial disturbance.

Figure 9 shows the surface-wave instability with $k = 0.7$, which is smaller than k_s. The linear growth rate is identical to that in the case shown in figure 5. In figure 9(*a*), each line represents a time increment of 0.05, with the final time step $\tau = 2$. As time increases, the amplitude of the disturbance at first increases exponentially, as in the previous cases of $k > k_s$, but soon grows super-exponentially; even higher harmonics are excited in the initial instability stage. The local phase speed of the wave increases with the local layer thickness. Therefore, this super-exponential growth makes the crests travel significantly faster than the troughs, resulting in steepening of the front and incipient wavebreaking.

In figures 5–9, differences in local growth rate are seen; the thinning at the trough is much slower than the growth at the crest. This can be understood by examining the vertical component (3.9) of the velocity at the free surface; the driving forces depend on powers of h and, hence, act more effectively on thicker regions. This phenomenon, that the positive deviation from the mean film thickness is more pronounced than the negative one, seems to be typical for gravity-driven viscous flows. Yiantsios & Higgins (1989) examined Rayleigh–Taylor instability in thin viscous films and saw a similar phenomenon.

It is thus seen that the surface-wave instability causes a rapid growth of the crest, a steepening of the slope behind the trough. When the initial disturbance wavenumber is large (but small enough to cause the instability), the disturbance

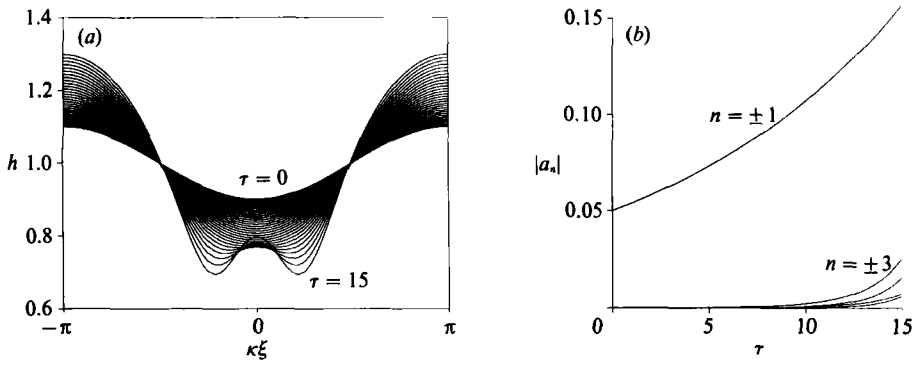

FIGURE 10. Free-surface evolution for a thermocapillarity instability in the absence of gravity. $k = 0.7$ ($k_M = 2.03$), $KM/P = 1, K = 0.1, \bar{S} = 0.1$: (*a*) free-surface configurations with $\Delta\tau = 0.5$ up to $\tau = 15$; (*b*) evolution of the spectral coefficients.

equilibrates after initial growth and steepening. When the initial disturbance wavenumber is small, the evolution via (3.13) is highly unstable and the continuous growth of the crest and the steepening can lead to wavebreaking. The thinning of the trough is slow, and the wavebreaking is likely to occur before the trough thins significantly. Therefore, the surface-wave instability by itself does not easily initiate film rupture and dryout.

6.2. *Layers with thermocapillarity* ($G, \bar{S}, K, KM/P \neq 0; \bar{E} = E^2/D = 0$)

We now examine the evolution of a non-volatile layer on a heated plate. The thermocapillarity described by (3.13) models the long-wave instability that occurs when the free surface is deformable. The effects of thermal convection are small, and the instability is induced by vertical temperature gradients in the layer and differences in the local layer thickness that generate temperature differences along the interface.

There is another mode of instability that exists when thermal convection is significant. Pearson (1958) showed for $\bar{S} \to \infty$ (non-deformable surface) that the onset of this instability occurs when the wavelength is of order unity (compared to the layer depth). Goussis & Kelly (1990) allow surface deformation and find a sufficient condition that this unit-order wavenumber instability is absent. This criterion, valid for $G \gg 1$, states that all thermocapillary instabilities have small wavenumber if, in our notation, $KM > 16.037$. When G decreases, the allowable values for M increase, so that these instabilities are less likely. In the cases shown below, for which $G = M = O(1)$, as required by (3.13), we have $K = 0.1$, so that only the long-wave instability is present.

Figures 10 and 11 show the unstable evolution of a thin layer in the absence of gravity ($G = 0$). It corresponds to the point P2 in figure 3 with $KM/P = 1$, $K = 0.1$ and $\bar{S} = 0.1$. The cutoff wavenumber $k_c \approx 2.87$, the maximizing wavenumber $k_M = 2.03$. Two different initial instabilities wavenumbers are chosen: $k = 0.7$ in figure 10 and $k = k_M$ in figure 11.

In figure 10(*a*), each line represents the free-surface configuration for τ increments of 0.5, and the last state shown is at $\tau = 15$, in which there is a characteristic 'two-finger' shape. In the initial stage, the disturbance grows exponentially, as predicted by linear theory. Energy is confined to the unstable fundamental mode, and thus the free surface keeps its simple harmonic configuration. As the amplitude grows, the free surface near the trough flattens due to the 'thin-layer' mentioned above. Since the

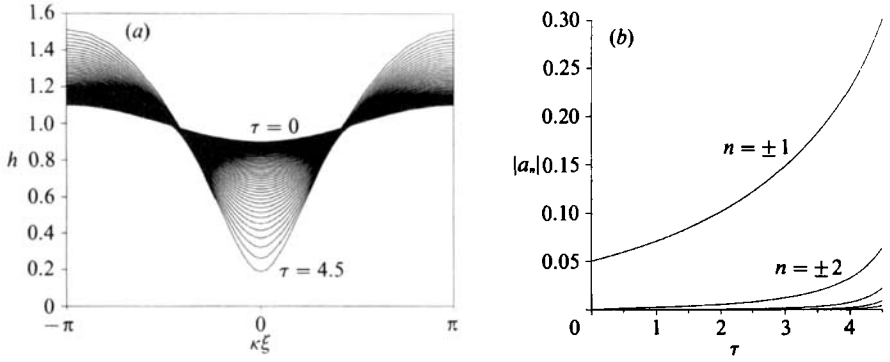

FIGURE 11. Free-surface evolution for a thermocapillarity instability in the absence of gravity. $k = k_M$, $KM/P = 1$, $K = 0.1$, $\bar{S} = 0.1$: (*a*) free-surface configurations with $\Delta\tau = 0.5$ up to $\tau = 4.5$; (*b*) evolution of the spectral coefficients.

two edges of the flattened region have large slope and positive curvature, they are rapidly drawn downwards by capillary pressures: the pressure in the liquid is lower near the edges than near the flattened region in the centre. This creates both a draining outward and a characteristic bulge in the centre. The destabilizing thermocapillary effect induces large velocities toward the plate, though at the centre the growth is almost zero; the edges bulge downward, resulting in the growth of the new troughs. As this process develops, the fluid near the centre is trapped between the new troughs, since high-pressure regions are located on each side of them. The centre then moves upward in order to conserve mass, and acts as a new upward-growing crest. At this stage, the energy is no longer confined to the fundamental mode but has spread into its harmonics, as seen in figure 10(*b*). The modes $n = \pm 3$ have the largest growth rate according to the linear theory, and are the most pronounced among the harmonics. Unlike the surface-wave instability for isothermal layers, the fundamental mode continues to grow as the instability develops, and so is dominant through $\tau = 15$. Beyond $\tau = 15$, the long-wave assumption is violated as the higher harmonics become important. In contrast to the behaviour of isothermal layers, there is no substantial difference in local growth rates of the crests and the troughs until the secondary dimples appear. As can be seen from (3.9), the growth driven by thermocapillarity alone is not as sensitive to the local thickness of the layer as is the surface-wave mode. In fact, the thinning rate at the trough is slightly larger than the growth rate at the crest, because the thickness-dependent stabilizing effect of mean surface tensions acts more strongly on the crests.

If we take larger values for the initial disturbance wavenumber k, the linear growth rate of the fundamental mode relative to its harmonics increases. In nonlinear evolution, the flattening of the trough and the 'fingering' are delayed until the trough thins further. In figure 11, we take $k = k_M$. As shown in the free-surface configuration for each τ increment of 0.1 in figure 11(*a*), the 'fingering' does not occur until the trough thins to below approximately 20% of its initial thickness. Further computations, not given here, show that the flattening of the trough occurs at about $\tau = 4.6$ and the 'fingering' develops subsequently. For times larger than $\tau = 4.5$, however, the Fourier spectrum broadens to include modes outside the long-wave theory. In figure 11(*b*), the magnitudes of the five lowest modes are plotted up to $\tau = 4.5$. The fundamental mode ($n = \pm 1$) corresponds to the linear maximum growth rate, and grows more rapidly than its harmonics. The harmonics eventually become important, and the 'fingering' would occur before the layer ruptures.

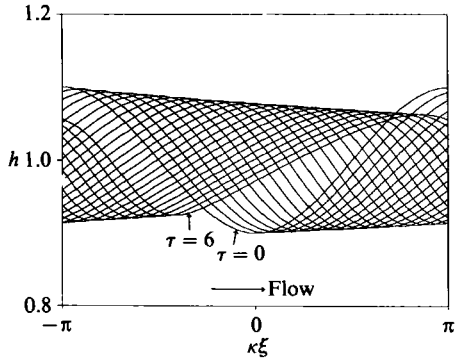

FIGURE 12. A stable evolution of a free surface with hydrodynamic and thermocapillary effects. $k = 0.7$, $G = 5$, $\beta = 10°$, $KM/P = 1$, $K = 0.1$, $\bar{S} = 0.1$ with $\Delta\tau = 0.5$ up to $\tau = 6$.

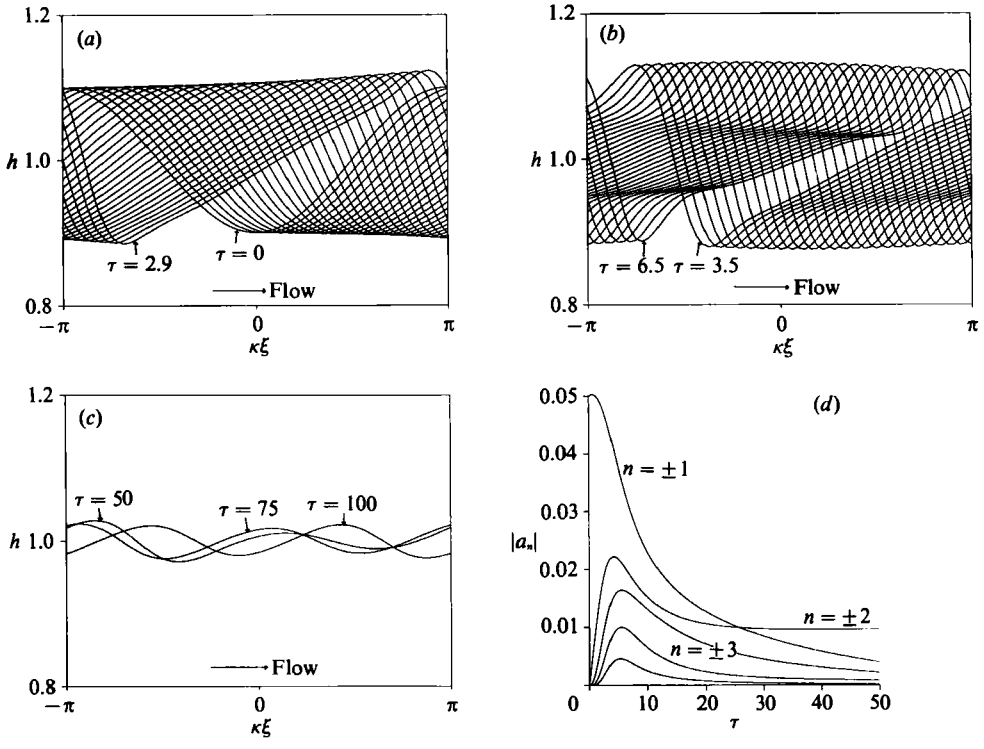

FIGURE 13. Evolution of the free-surface configuration when $k = 0.7$ ($k_M = 1.04$), $G = 5$, $\beta = 30°$, $KM/P = 1$, $K = 0.1$, $\bar{S} = 0.1$: (*a*) $0 \leqslant \tau \leqslant 2.9$ with $\Delta\tau = 0.1$; (*b*) $3.5 \leqslant \tau \leqslant 6.5$ with $\Delta\tau = 0.1$; (*c*) $\tau =$ 50, 75, and 100; (*d*) evolution of the spectral coefficients.

Figure 12 shows the same layer as in figure 10, but with gravity-induced mean flow and hydrostatic pressure gradient, $G = 5$ and $\beta = 15°$. This case corresponds to P3 in figure 3, which lies in the stable region Σ_S, where the thermocapillary instability is suppressed by hydrostatic pressure. The time increment for each configuration shown is 0.5, and the last configuration is at $\tau = 6$. The evolution shows monotonic decay of the disturbance. The local decay rates at crests and troughs look almost the same. However, the local phase velocity is higher at the crest than at the trough, owing to the viscous shear caused by the bottom. Consequently, the free-surface

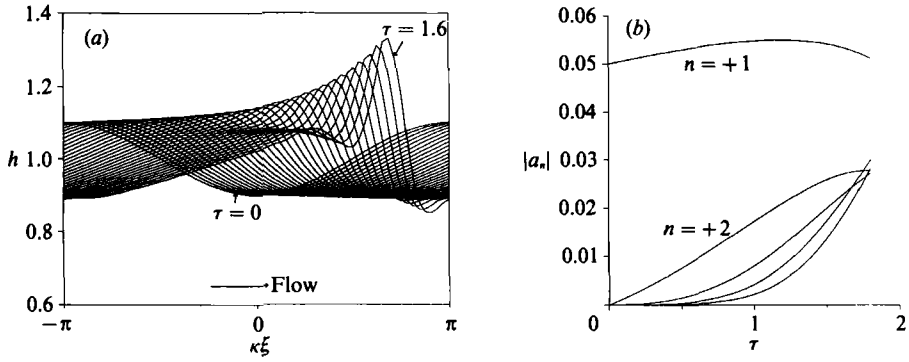

FIGURE 14. Evolutions with surface-wave and thermocapillary instability. $G = 5$, $\beta = 45°$, $KM/P = 1$, $K = 0.1$, $\bar{S} = 0.1$, and $k = 0.7$ ($k_M = 2.56$): (*a*) free-surface configurations with $\Delta\tau = 0.5$ up to $\tau = 1.6$; (*b*) evolution of the spectral coefficients.

configuration changes from its initial harmonic shape; the region behind the crest becomes flatter, while the region behind the trough barely changes shape.

If we now increase the angle of inclination to 30°, corresponding to P4 in figure 3, the flow becomes linearly unstable since the hydrostatic pressure is decreased. The corresponding isothermal film is stable, but thermocapillarity creates instability. Surface shapes for this case are shown in figure 13 for several different ranges of time and compare with those in figure 10. The wavenumber remains $k = 0.7$, and $k_M = 1.04$. Figure 13(*a*) shows the evolution for $0 \leqslant \tau \leqslant 2.9$ with $\Delta\tau = 0.1$. The unstable fundamental mode grows with time, so that the disturbance amplitude increases, in agreement with the linear theory. As the instability develops, however, the fundamental mode starts to lose its energy, as shown in figure 13(*b*) ($3.5 \leqslant \tau \leqslant 6.5$). It appears that the disturbance tends toward a permanent wave rather than wavebreaking or fingering, as is seen in figure 13(*c*). The evolution of spectral coefficients shown in figure 13(*d*) indicates that the modes $n = \pm 2$ eventually dominate. Therefore, the equilibrated state would have a dominant wavenumber twice that of the initial state, as shown in figure 13(*c*).

In figure 14, the angle of inclination is further increased to 45°. This corresponds to P5 in figure 3; separately, there is the surface-wave instability shown in figures 5–9 and the thermocapillary instability of figure 10. Each instability is amplified by the interaction with the other. Here, $k = 0.7$ as in figure 9, while $k_M = 2.56$ and $k_c = 3.63$. As the wave travels down the plate, a surface-wave instability evolves similar to that of the isothermal film. The growth rate is higher, so that dimples appear earlier. Once the dimple appears, the thermocapillary effect acts strongly upon it and enhances the secondary developments, which in turn rapidly steepens the wave and (presumably) causes wavebreaking at an earlier time. As seen in figure 14(*b*), the harmonics grow more rapidly than those in figure 9(*b*) due to the thermocapillarity.

For isothermal layers, as k is increased the nonlinear interactions become weaker, and the secondary flow eventually equilibrates for sufficiently large k. When thermocapillarity is present, however, the thermocapillary instability can prevent the equilibration. An example is shown in figure 15, where $k = 1.56$ as in figure 6. Initially, the surface-wave instability is dominant, so that the evolution is similar to that of the isothermal layer. Soon the thermocapillary instability becomes effective, and enhances the growth of the disturbance. Instead of the equilibration, the evolution in figure 15(*b*) shows 'catastrophic' growth as in figure 8(*e*). The spectral coefficients plotted in figure 15(*c*) clearly show that equilibration does not occur.

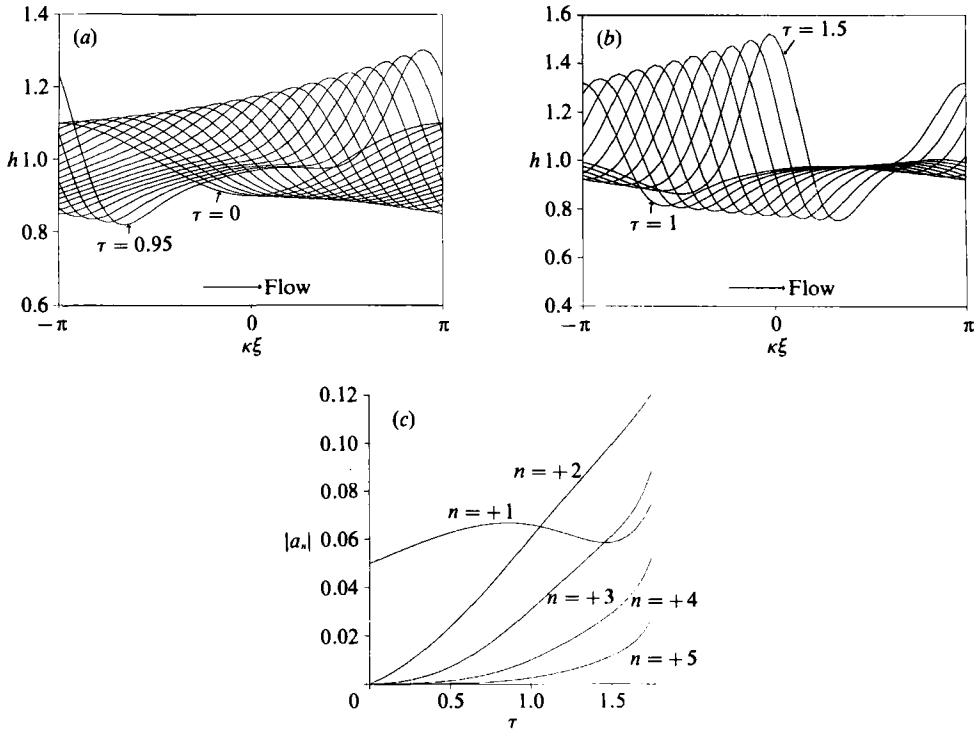

FIGURE 15. Evolutions with surface-wave and thermocapillary instability. $G = 5$, $\beta = 45°$, $KM/P = 1$, $K = 0.1$, $\bar{S} = 0.1$, and $k = 1.56$: (*a*) free-surface configurations for $0 \leqslant \tau \leqslant 0.95$ with $\Delta\tau = 0.05$; (*b*) free-surface configurations for $1 \leqslant \tau \leqslant 1.5$ with $\Delta\tau = 0.05$; (*c*) evolution of the spectral coefficients.

Other computations near $k = k_c$ also show no equilibration. The surface configurations are closer to the monochromatic wave, but the continuous growth of the fundamental induces 'catastrophic' behaviour.

In figure 16, a stronger thermocapillary effect is considered ($KM/P = 5$), one which can overcome the stabilizing hydrostatic pressure even when the plate is horizontal ($G = 5$, $\beta = 0°$). Unstable evolutions are shown for several different angles of inclination with $\Delta\tau = 0.05$ and $k = 0.7$. Figure 16(*a*) shows the evolution of the instability on a horizontal plate. As in figure 10, the disturbance amplitude grows and then secondary instability starts. The growth at the crest, however, is distinctively slower than that at the trough, in contrast to the case with the hydrostatic pressure absent. In figure 16(*b*) the plate is tilted to $\beta = 10°$, and so the liquid is flowing. Again, the crest is moving faster than the trough, steepening the slope behind the trough. Therefore, when the trough flattens and the edges bulge outwards, the rear edge has the larger curvature. It then grows down faster than the other due to thermocapillarity. The secondary 'finger', is not swept downstream substantially by the flow but grows vertically downward. In figures 16(*c*) and 16(*d*) the angle of inclination is set at 20° and 30°, respectively. As the angle increases, the effect of mean flow becomes more pronounced and the thermocapillary instability accordingly is enhanced. The steepening and the fingering tend to develop at earlier times. When $\beta = 45°$, the surface-wave instability is present. The two instability modes reinforce each other. In figure 16(*d*), the surface-wave mode is apparent first, so that significant steepening and secondary structures are seen before the fingering.

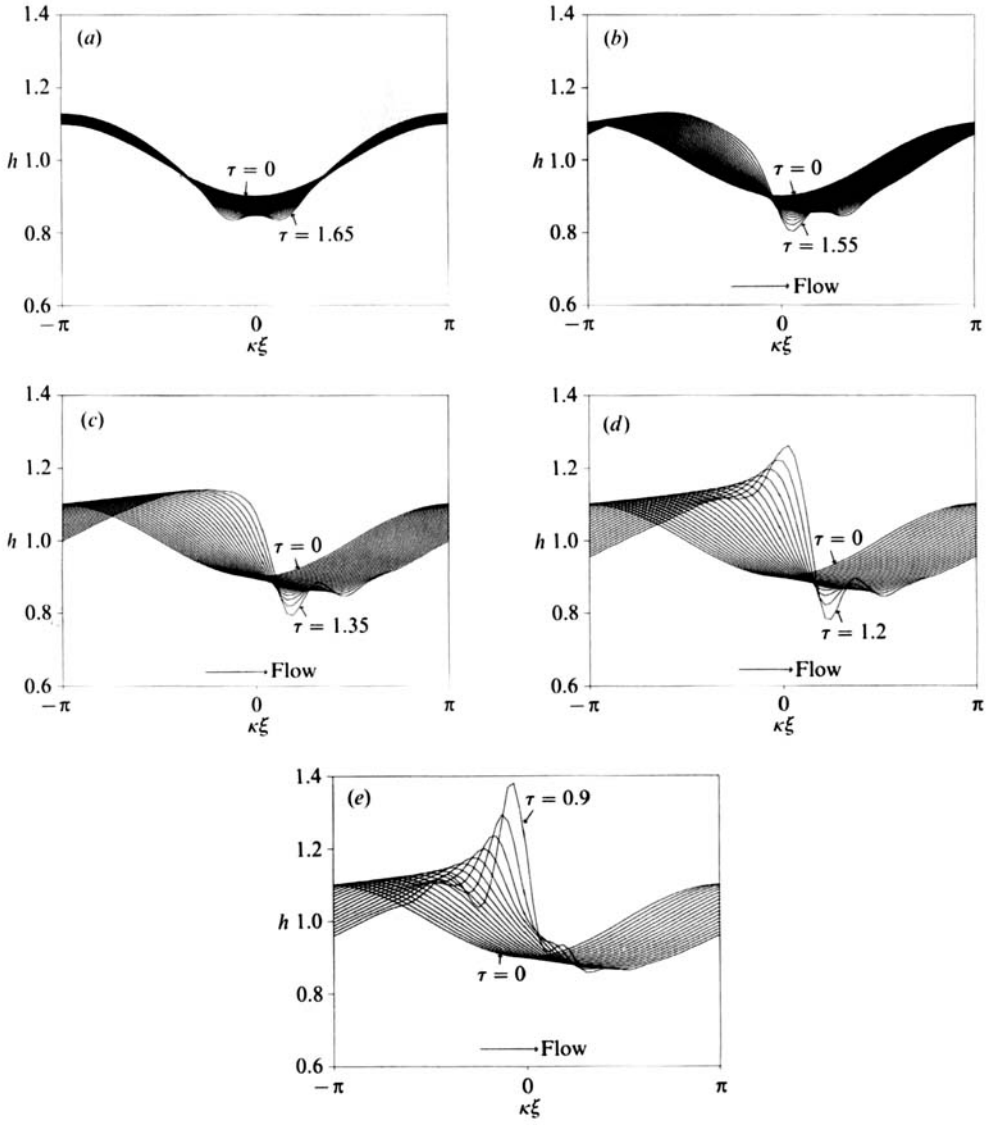

FIGURE 16. Evolution of the free-surface configuration when $k = 0.7$, $G = 5$, $KM/P = 5$, $K = 0.1$, $\bar{S} = 0.1$ with $\Delta\tau = 0.05$: (*a*) $\beta = 0°$ ($k_M = 3.51$); (*b*) $\beta = 10°$ ($k_M = 3.6$); (*c*) $\beta = 20°$ ($k_M = 3.84$); (*d*) $\beta = 30°$ ($k_M = 4.2$); (*e*) $\beta = 40°$ ($k_M = 4.6$).

Since the thermocapillarity is strong, no equilibration of the secondary flow (by taking k near k_c) is observed. In contrast to the evolution of the static layer, the growth of the crest is more pronounced owing to the mean flow.

One of the notable differences between the thermocapillary and surface-wave instabilities is the local growth rate of the trough as compared with that of the crest. The growth driven by surface-wave instability is more sensitive to the local layer thickness. For pure thermocapillary instability, however, the growth at the trough is comparable to that at the crest, so that it can cause significant local thinning of the layer.

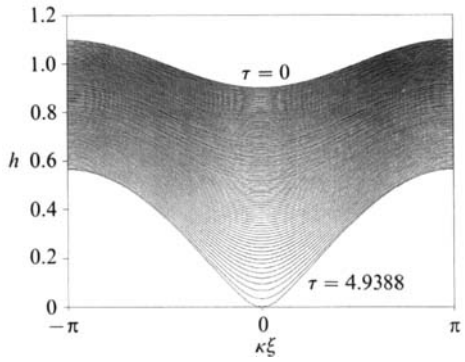

FIGURE 17. Free-surface profiles for an evaporating layer shown with $\Delta\tau = 0.05$ and at $\tau_R = 4.9388$. $k = 0.7$, $G = 0$, $\bar{E} = 0.1$, $K = 0.1$, $P = 1$, and $\bar{S} = 0.1$

6.3. *Evaporating layers* $(G, \bar{S}, \bar{E}, K, E^2/D, KM/P \neq 0)$

When there is evaporation, the basic-state layer thins and disappears at a finite time τ_D. When a disturbance is present, the trough will touch the heated plate before the basic state had disappeared. The effects of thermocapillarity and vapour recoil on the rupture instability have been discussed in detail by Burelbach *et al.* (1988). In this section we remark on this case but focus on the effects of gravity-driven flow and hydrostatic pressure.

Figure 17 shows a typical free-surface evolution for a purely evaporating film with surface tension ($\bar{E} = 0.1$, $\bar{S} = 0.1$, $P = 1$, $G = 0$, and $k = 0.7$). The surface profiles are shown for $\Delta\tau = 0.05$ and at the rupture time $\tau_R = 4.9388$. As seen in (3.12), the mass flux is smaller the larger the local thickness of the layer. Therefore, the liquid at the trough evaporates faster than the liquid elsewhere, which yields the configurations shown.

When vapour recoil is present, the film becomes unstable, as shown by the linear theory. The amplitude of the disturbance grows as the layer evaporates, resulting in a decrease in rupture time. The degree of decrease and the surface profiles depend on the relative timescales of the mass loss and the instability. When $\bar{E} \gg E^2/D$, the vapour recoil is weak, so that the decrease in rupture time is very small, and the surface profiles will be similar to those in figure 17. However, when $\bar{E} \ll E^2/D$, the vapour recoil is substantial, the rupture time is substantially decreased, and the surface profiles will have sharper troughs, and possibly more elevated crests. Burelbach *et al.* (1988) show the profiles for various choices of the parameters. In figure 18, the surface profiles with $\Delta\tau = 0.05$ and the corresponding evolution of a few lowest spectral coefficients are shown when $\bar{E} = 0.1$, $K = 0.1$, $E^2/D = 2$, $\bar{S} = 0.1$, and $G = 0$. Three different initial wavenumbers, $k = 0.5$, 0.7, and 1.0 ($k_M = 2.74$), are taken to show three distinct evolutions. Of the three, the linear growth rate is the smallest for $k = 0.5$ and the largest for $k = 1.0$. In figure 18(a, b) ($k = 0.5$) the contribution to the thinning of the trough from the instability is small, so that the surface configurations are similar to those in figure 17. However, the thinning rate near the trough is increased while that near the crest is decreased due to the evaporative instability. The rupture time thus is decreased to $\tau_R = 4.6425$. If k is increased to 0.7, the effective linear growth is larger. The contribution of the instability accordingly is increased, resulting in much more pronounced local depression at the trough near rupture, as seen in figure 18(c). The growth of the fundamental mode ($n = \pm 1$) in figure 18(d) is faster than that in figure 18(b). If we

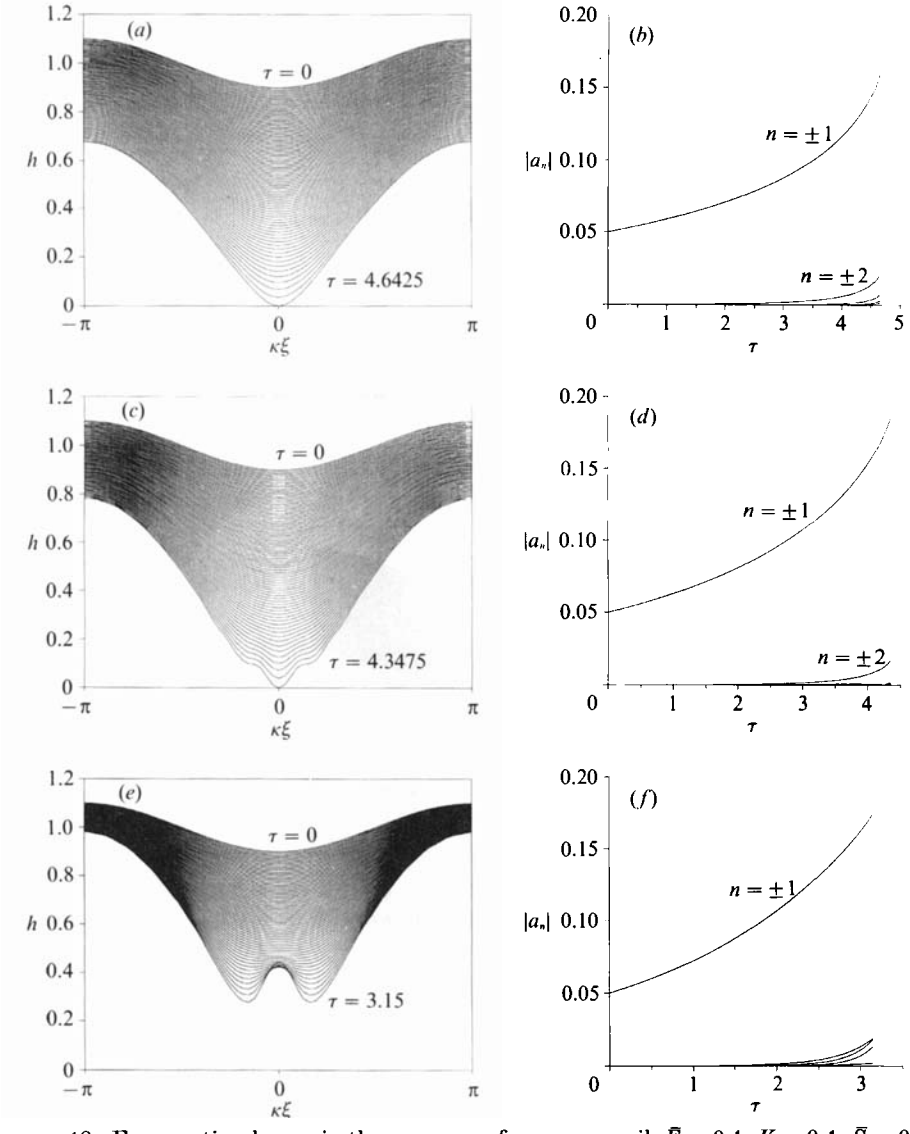

FIGURE 18. Evaporating layers in the presence of vapour recoil. $\bar{E} = 0.1$, $K = 0.1$, $\bar{S} = 0.1$, $P = 1$, and $E^2/D = 2$ ($k_M = 2.74$): (*a*) free-surface profiles for $k = 0.5$ with $\Delta\tau = 0.05$ and at $\tau_R = 4.6425$; (*b*) evolution of spectral coefficients for $k = 0.5$; (*c*) free-surface profiles for $k = 0.7$ with $\Delta\tau = 0.05$ and at $\tau_R = 4.3475$; (*d*) evolution of spectral coefficients for $k = 0.7$; (*e*) free-surface profiles for $k = 1.0$ with $\Delta\tau = 0.05$ up to $\tau = 3.15$; (*f*) evolution of spectral coefficients for $k = 1.0$.

further increase k toward k_M, the contribution of the instability to the local thinning of the layer increases. If k exceeds a certain critical value and the local thinning near the trough becomes sufficiently rapid, the liquid has to flow away from the trough in addition to evaporating. Therefore, the flattening of the trough and the fingering would occur before the layer ruptures. One such case is shown in figure 18(*e*, *f*) with $k = 1.0$. The evolution is shown up to $\tau = 3.15$, beyond which the local surface slope near the fingers becomes too large to be described by the long-wave theory. It appears that as the instability develops further, the finger tips would be drawn to the plate and so a two-point rupture is expected.

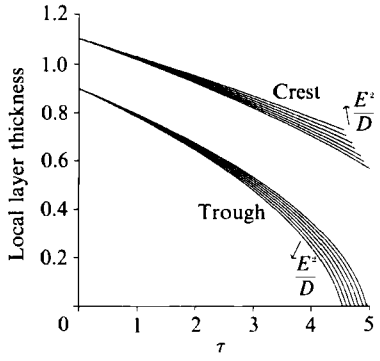

FIGURE 19. Evolution of crests and troughs for evaporating layers for several different values of vapour recoil. $k = 0.7$, $\bar{E} = 0.1$, $K = 0.1$, $\bar{S} = 0.1$, $P = 0$, and $0 \leqslant E^2/D \leqslant 1.5$ with equal increment of 0.25.

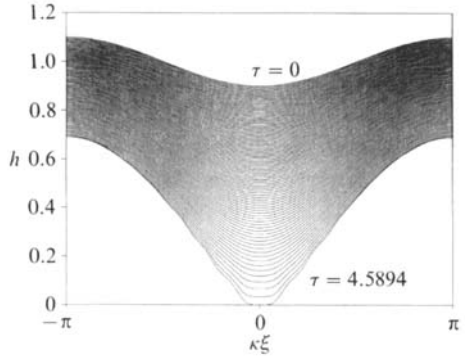

FIGURE 20. An evaporating layer with thermocapillarity. $k = 0.5$ ($k_M = 2.03$), $\bar{E} = 0.1$, $K = 0.1$, $\bar{S} = 0.1$, $P = 1$, and $KM/P = 2$. Free-surface profiles are shown with $\Delta\tau = 0.05$ and at $\tau_R = 4.5894$.

In figure 19, the local thicknesses of the layer at the crest and the trough are plotted against time until the layer ruptures. Several values for E^2/D are considered between 0 and 1.5, while $\bar{E} = 0.1$, $K = 0.1$, $P = 0$ and $\bar{S} = 0.1$ as in figure 17. For all cases, the thinning rate of the trough is larger than that of the crest. As the effect of vapour recoil increases, the thinning rate of the trough increases and that of the crest decreases. In the range of the parameters taken, the rupture time decreases linearly with E^2/D.

The thermocapillary instability for this evaporating layer can have interesting effects on rupture. Primarily, this instability accelerates the rupture, and thus the rupture time will decrease with KM/P, as for the evaporative instability. When the fingering occurs before the layer ruptures, the location of rupture may be changed as in figure 18(*e*). This two-point rupture will occur when KM/P is sufficiently large compared to $\bar{E}$, and k is sufficiently close to k_M to provide rapid growth of the initial disturbance. In figure 20, $k = 0.5$ ($k_M = 2.03$), $\bar{E} = 0.1$, $K = 0.1$, and $KM/P = 2$. Surface profiles are shown at $\Delta\tau = 0.05$ and at rupture, $\tau_R = 4.5894$. As the layer thins, the trough flattens and touches the plate. When k is somewhat smaller than 0.5, the surface profiles are closer to those in figure 17 with slightly larger τ_R. On the other hand, if k is somewhat larger than 0.5, the two-point rupture is observed.

Figure 21 shows the evolution of the evaporating film of figure 17 with mean-flow

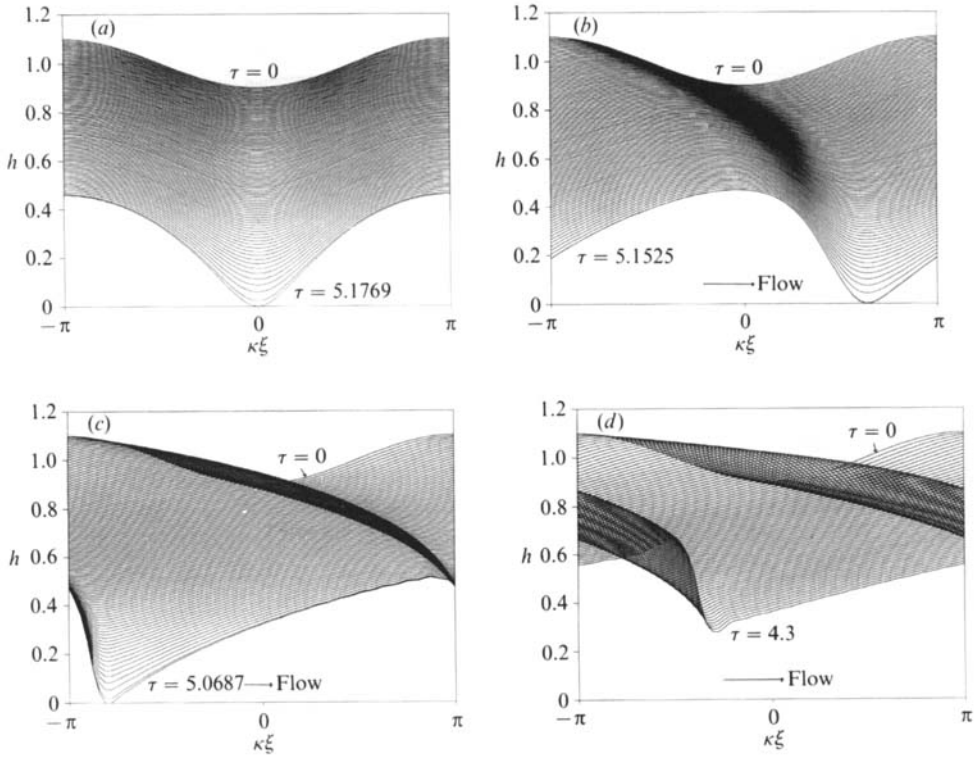

FIGURE 21. Evaporating layers with gravitational effects. $k = 0.7$, $\bar{E} = 0.1$, $K = 0.1$, $P = 1$, $\bar{S} = 0.1$, and $G = 5$. Free-surface profiles are shown with $\Delta\tau = 0.05$: (*a*) $\beta = 0°$ and $\tau_R = 5.1769$; (*b*) $\beta = 15°$ and $\tau_R = 5.1525$; (*c*) $\beta = 30°$ and $\tau_R = 5.0687$; (*d*) $\beta = 45°$ and $\tau = 4.3$.

effects added. Here $k = 0.7$, $G = 5$, and the angle of inclination is varied from zero to 45°. Surface profiles are shown at $\Delta\tau = 0.05$ and at τ_R. When the plate is horizontal, the hydrostatic pressure stabilizes the flow and tends to flatten the film. Therefore, τ_R is increased to 5.1769, and the difference in local thickness at the crest and the trough is much smaller than that in figures 17 and 18.

When the plate is tilted to 15°, the disturbance wave travels down the slope, and thus the location of rupture is shifted downstream. Without the evaporation, the flow would be stable and so the surface would tend to $h = 1$. However, because of evaporation, the trough is drawn to the plate faster than the crest. This amplification of the local-thickness difference causes a difference in local phase speed, so that the crest travels faster than the trough. Therefore, near rupture the surface behind the trough is steepened considerably. The rupture time $\tau_R = 5.1525$ is again larger than that in figure 17, but has been slightly decreased from that in figure 21(*a*) because the hydrostatic forces have been decreased by the tilting.

The steepening of the surface and the decrease in rupture time due to tilting are more clearly seen in figure 21(*c*), where the angle of inclination is 30°. Without evaporation, the flow would be stable. The rupture time is reduced to $\tau_R = 5.0687$, and the difference in the local phase speeds is much larger. Accordingly, near rupture the surface behind the trough becomes very steep, and that behind the crest is stretched. After the rupture, it can be expected that the liquid layer behind the rupture point rolls over before a dry region could expand significantly. Under certain conditions, re-wetting may be followed by a second rupture, a second re-wetting, and

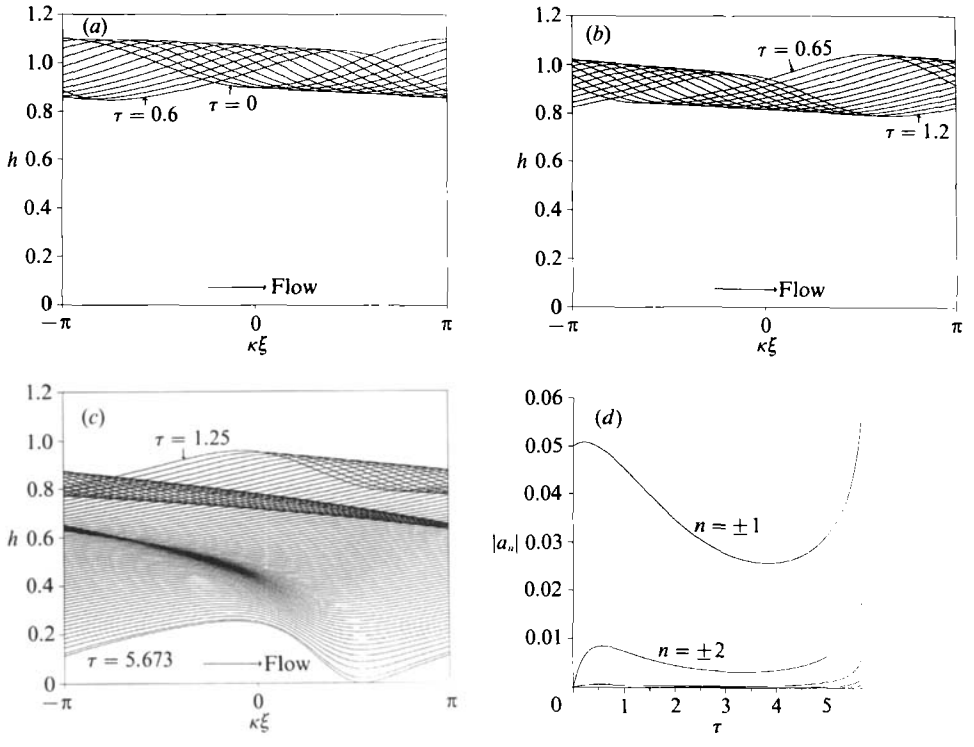

FIGURE 22. Evaporating layers with surface-wave instability. $k = 2.1$, $\bar{E} = 0.1$, $K = 0.1$, $P = 1$, $\bar{S} = 0.1$, and $G = 5$. Free-surface profiles are shown with $\Delta\tau = 0.05$: (*a*) for $0 \leqslant \tau \leqslant 0.6$; (*b*) for $0.65 \leqslant \tau \leqslant 1.2$; (*c*) for $1.25 \leqslant \tau \leqslant 5.673$; (*d*) evolution of the spectral coefficients.

so on. Therefore, when a layer falls down an inclined plate a number of rupture/re-wetting processes may be possible before it evaporates completely.

Figure 21(*d*) corresponds to a case in which the surface-wave instability causes wavebreaking before the layer ruptures. The angle of inclination is 45°, and the surface profiles are shown up to $\tau = 4.3$, beyond which the surface behind the trough steepens rapidly and the evolution equation (3.13) loses validity. The corresponding isothermal instability is shown in figure 9, which indicates wavebreaking at a much earlier time. The wave propagation is retarded owing to evaporation. As the instability grows, the surface behind the crest is stretched and becomes almost flat.

If we consider the same layer as in figure 21(*d*) but change the wavenumber k, different behaviour will be obtained, because the corresponding isothermal layer is very sensitive to k, as shown in figures 5–9. When k is sufficiently large, the wavebreaking is not likely to occur before rupture. In figure 22 one such example is shown for $k = 2.1$ ($k_c \approx 2.21$). The surface profiles for different time ranges with $\Delta\tau = 0.05$ are shown separately in figures 22(*a*)–22(*c*) for clarity. The spectral coefficients are plotted in figure 22(*d*) for comparison with figure 5(*c*). After the initial surface-wave instability the harmonics decay as for the isothermal layers, but the equilibration is prevented by the evaporation.

As seen in figure 21, a significant effect of the mean flow on evaporating layers is the creation of wavebreaking. When the surface-wave instability is present with small enough k, the incipient wavebreaking occurs before the trough touches the plate, resulting in a significant delay in rupture time. When k is close to k_c, as in

figure 22, the wavebreaking does not occur. However, substantial steepening can occur, in contrast to the corresponding evolution without the mean flow. This steepening is observed also for layers without the surface-wave instability (figure 21*b*, *c*). When the layer ruptures with significant steepening, the fluid behind may break over the dry spot and the rupture/re-wetting processes may occur and even be repeated. The surface-wave instability may accelerate the rupture, but in most cases the instability does not accompany significant depression of the trough before the wavebreaking, as shown and discussed in figure 9.

7. Discussion and conclusions

The present work examines falling films of liquid on heated inclined planes. It includes viscous, pressure, gravity, capillary, and thermocapillary forces. If the liquid is volatile, it allows for the mass loss and vapour recoil of thermal evaporation. The long-wave evolution equation for the interface shape, which is derived for two-dimensional disturbances, is asymptotically equivalent to the original free-boundary problem. This extends the equation of Burelbach *et al.* (1988) to unit-order P and M, retains $O(\epsilon)$ corrections, and generalizes this to gravity-driven layers.

The evolution equation possesses two simple solutions. (i) There is a time-dependent spatially uniform layer that corresponds to an infinite layer that thins due to evaporation. (ii) There is also a steady-state spatially tapering layer that is finite; it begins at $x = 0$, thins in the flow direction, and terminates at a contact line. The mass flow at the entrance is balanced by the evaporative flux through the interface. Both of these are physically realizable states but only the stability of the former state, spatially uniform and thinning, is treated herein.

The isothermal layer is susceptible to surface-wave instabilities. Linear theory supplies the critical Reynolds number and corresponding phase speed. The phase speed depends directly on the square of the local layer thickness and so there is a built-in tendency for wavebreaking as is seen in the nonlinear analysis. The nonlinear behaviour of the layer is very sensitive to the initial disturbance wavenumber. When the disturbance wavenumber is sufficiently small, numerical solution of the evolution equation shows that the wave initially grows at the exponential rate of linear theory, but soon grows super-exponentially. The peaks grow much faster than the troughs deepen, and the front of the peaks steepens towards the vertical, showing incipient breaking, and a secondary trough grows behind the peak. The wave breaks faster than the trough depresses, so that here dryout is not likely to occur. Quantitative analysis of the wavebreaking is beyond the scope of the present work, because the evolution loses its validity as the maximum local slope of the free surface exceeds $O(1/\epsilon)$. When the disturbance wavenumber is closer to the cutoff value k_c, the flow becomes supercritically equilibrated after the initial instability. The surface wave then approaches a permanent form, as observed in experiments. Different initial states give different equilibrium states.

The non-isothermal layer of non-volatile liquid is susceptible to thermocapillary instabilities. Linear theory supplies the critical Marangoni number, as shown in figures 2 and 3. When the plate is horizontal, thermocapillary and hydrostatic effects compete. When the plate is tilted, there is a mean flow that produces surface waves. When the effective Marangoni number $\mathcal{M}$ is large enough (see figure 3), changes in G can either stabilize or destabilize the basic state. This state is stable at point P3 of figure 3. If G is increased to P4, surface waves, as modified by thermocapillarity, will grow. If G is at P3 and lowered to P2, thermocapillary instability will be present.

As G is increased from P2, gravity effects will be introduced and finally, as G increases towards P3, the hydrostatic pressure will stabilize the layer, as we have seen earlier. The existence of this window of stability for falling films with thermocapillarity was first noticed and discussed by Kelly *et al.* (1986). The phase speed is not affected by thermocapillarity. In contrast to isothermal layers, the local growth rate at the trough driven by thermocapillarity is comparable to that at the crest, so that significant local thinning of the layer can be expected. In the initial stage, the disturbance grows exponentially, as predicted by linear theory. As the amplitude grows, the trough tends to flatten, owing to capillary pressure. Thermocapillarity then acts strongly on the edges of the flattened region, so that the edges bulge downward, resulting in the growth of new troughs. The flat region in the centre stops growing and then moves upward in order to conserve mass. When the disturbance wavenumber k is small, this 'fingering' occurs at an early stage, but as k increases it is delayed until the trough thins significantly. For horizontal layers, the development of the fingers is symmetric.

For layers on a tilted plate, the effects of mean flow are present. When there is no surface-wave instability and the thermocapillarity is weak, the flow equilibrates after initial instability. When the thermocapillarity is strong enough, the disturbance grows continuously and the layer tends to rupture. When the fingering occurs, the upstream finger maintains the larger curvature due to the steepening of the front, and thus grows downwards faster. When the surface-wave instability is present, the thermocapillarity enhances the instability and promotes the wavebreaking. The equilibration seen for isothermal layers does not occur when both instabilities are present.

The non-isothermal layer of volatile liquid is susceptible to vapour recoil, thermocapillary, and wavebreaking instabilities. Linear theory supplies the critical value of E^2/D, as shown in figures 2 and 3. As in the case of the non-volatile liquid, there is a window of stability above which and below which the basic state is unstable. When vapour recoil or thermocapillarity is present, the instability can be accompanied by significant local thinning of the layer, resulting in a decrease in rupture time.

When the mean flow is present, the interface steepens. If significant steepening occurs before rupture, wavebreaking may follow the rupture. When surface-wave instability is present and the disturbance wavenumber is small enough, wavebreaking will occur before rupture. Therefore, the mean flow can either retard the rupture or cause the rewetting of the dry region.

If the trough of a disturbed layer becomes as thin as 1000 Å, van der Waals attractions may drive the region to rupture (see Ruckenstein & Jain 1974; Williams & Davis 1982; Burelbach *et al.* 1988). For simplicity, such forces have been omitted in the present analysis, but can easily be incorporated, as seen in (7.1) below. Clearly, the dryout criteria derived in this paper would be modified by the presence of van der Waals attractions.

One of the functions of long-wave theory for thin films is to unify, here in a single evolution equation, the effects of several instabilities and their couplings. Not only does it give quantitative predictions as discussed above but it also helps identify new phenomena even in cases where the solutions break down after a finite time. We have seen here the existence of a window of instability, the presence of incipient wavebreaking and permanent waves, the 'two-finger' thinning process, the promotion of breaking by heat transfer, the possible bypassing of dryout by flow of breaking waves 'filling in' the depressions, the promotion of dryout by flow when

simultaneous instabilities are present, and the destruction of permanent waves by mass loss. The theory identifies parameter value where one or another coupling can occur.

Many of the competitions studied here are in principle sensitive to the fact that we have allowed only two-dimensional instabilities. Some of the flow structures may be modified in three dimensions since there can be flow around them. Thus, steepening of waves may be weakened and dry patches may become independent of streamwise direction. Clearly, three-dimensional effects are of great importance and are the subject of subsequent studies. The extended evolution equation can be written down directly as shown below.

We now allow three-dimensional disturbances and include long-range molecular forces, with the y-coordinate directed cross-stream, and with A as a measure of the van der Waals attractions, as detailed by Burelbach *et al.* (1988). A straightforward extension of (3.13) gives

$$h_\tau + \frac{\bar{E}}{h+K} + Gh^2 h_\xi \sin\beta + \epsilon \frac{2G^2}{15}(h^6 h_\xi)_\xi \sin^2\beta$$
$$+ \epsilon \nabla \cdot \left\{ \left[\frac{KM}{P}\left(\frac{h}{h+K}\right)^2 + \frac{E^2}{D}\left(\frac{h}{h+K}\right)^3 - \tfrac{1}{3}Gh^3\cos\beta + \frac{A}{h} \right] \nabla h + \bar{S}h^3 \nabla(\nabla^2 h) \right\}$$
$$+ \epsilon \bar{E} \frac{5G}{24}\left\{ \frac{h^4}{h+K} \right\}_\xi \sin\beta + \epsilon \bar{E} P \left(\frac{h}{h+K}\right)^3 \left[\frac{\bar{E}}{3(h+K)} + \frac{G}{120}(7h-15K)\, h h_\xi \sin\beta \right] = 0. \quad (7.1)$$

Here ∇ is the gradient operator $(\partial_\xi, \partial_\eta)$, where $\eta = \epsilon y$. Then, the effective growth rate $\Gamma^{(3D)}$ from linear theory becomes

$$\Gamma^{(3D)} = \epsilon \left[\frac{E^2}{D}\left(\frac{h_0}{h_0+K}\right)^3 + \frac{KM}{P}\left(\frac{h_0}{h_0+K}\right)^2 + \frac{A}{h} - \frac{G}{3}h_0^3 \cos\beta \right] k^2$$
$$+ \epsilon k^2 \cos^2\theta \frac{2G^2}{15} h_0^6 \sin^2\beta - \epsilon \bar{S} h_0^3 k^4, \quad (7.2)$$

where k is now the magnitude of the wavenumber vector $\boldsymbol{k} = (k\cos\theta, k\sin\theta)$ on the (ξ, η)-plane. It can be easily shown from the above relationship that for a given k two-dimensional disturbances along the incline ($\theta = 0$) are more unstable in the linear theory than are oblique disturbances; this is a generalization of Squire's theorem.

The authors are indebted to Professor H. True, who participated in the early formulation and analysis of the evolution equation. The authors gratefully acknowledge Professor W. W. Schultz for valuable discussions. This work was supported by US Department of Energy, Division of Basic Energy Sciences, through Grant no. DE FG02-86ER13641.

REFERENCES

ATHERTON, R. W. & HOMSY, G. M. 1976 On the derivation of evolution equations for interfacial waves. *Chem. Engng Commun.* **2**, 57–77.

BANKOFF, S. G. 1971 Stability of liquid flow down a heated inclined plane. *Intl J. Heat Mass Transfer* **14**, 377–385.

BENJAMIN, T. B. 1957 Wave formation in laminar flow down an inclined plane. *J. Fluid Mech.* **2**, 554–574.

BENNEY, D. J. 1966 Long waves on liquid films. *J. Math. & Phys.* **45**, 150–155.

BURELBACH, J. P., BANKOFF, S. G. & DAVIS, S. H. 1988 Nonlinear stability of evaporating/condensing liquid films. *J. Fluid Mech.* **195**, 463–494.

CHANG, H.-C. 1989 Onset of nonlinear waves of falling films. *Phys. Fluids* A **1**, 1314–1327.

DAVIS, S. H. 1983 Rupture of thin liquid films. In *Waves in Fluid Interfaces* (ed. R. E. Meyer), pp. 291–302. Academic.

GJEVIK, B. 1970 Occurrence of finite-amplitude surface waves on falling liquid films. *Phys. Fluids* **13**, 1918–1925.

GOUSSIS, D. A. & KELLY, R. E. 1990 On the thermocapillary instabilities in a liquid layer heated from below. *Intl J. Heat Mass Transfer* **33**, 2237–2245.

KAPITZA, P. L. & KAPITZA, S. P. 1949 Wave flow of thin layers of a viscous fluid. *Zh. Ek. Teor. Fiz.* **19**, 105; also in *Collected Works*, pp. 690–709. Pergamon (1965).

KELLY, R. E., DAVIS, S. H. & GOUSSIS, D. A. 1986 On the instability of heated film flow with variable surface tension. *Proc. 8th Intl Heat Transfer Conf.*, vol. 4, pp. 1937–1942. (ed. C. L. Tien, V. P. Carey and J. K. Ferrell). Hemisphere.

KRANTZ, W. B. & GOREN, S. L. 1971 Stability of thin liquid films flowing down a plane. *Indust. Engng Chem. Fund.* **10**, 91–101.

LIN, S.-P. 1974 Finite amplitude side-band stability of a viscous film. *J. Fluid Mech.* **63**, 417–429.

LIN, S.-P. & WANG, C.-Y. 1985 Modeling wavy film flows. In *Encyclopedia of Fluid Mechanics*, vol. 1, pp. 931–951. Gulf Publishing Co.

PALMER, H. J. 1976 The hydrodynamic stability of rapidly evaporating liquids at reduced pressure. *J. Fluid Mech.* **75**, 487–511.

PEARSON, J. R. A. 1958 On convection cells induced by surface tension. *J. Fluid Mech.* **4**, 489–500.

PUMIR, A., MANNEVILLE, P. & POMEAU, Y. 1983 On solitary waves running down an inclined plane. *J. Fluid Mech.* **135**, 27–50.

RUCKENSTEIN, E. & JAIN, R. K. 1974 Spontaneous rupture of thin liquid films. *J. Chem. Soc. Faraday Trans. II* **70**, 132–147.

SPINDLER, B. 1982 Linear stability of liquid films with interfacial phase change. *Intl J. Heat Mass Transfer* **25**, 161–173.

SPINDLER, B., SOLESIO, J. N. & DELHAYE, J. M. 1978 On the equations describing the instabilities of liquid films with interfacial phase change. In *Two-Phase Momentum, Heat and Mass Transfer in Chemical Process and Energy Engineering Systems* (ed. F. Durst, G. V. Tsiklauri & N. H. Afgan), vol. 1, pp. 339–344. Hemisphere.

SREENIVASAN, S. & LIN, S.-P. 1978 Surface tension driven instability of a liquid film flow down a heated incline. *Intl J. Heat Mass Transfer* **21**, 1517–1526.

TOUGOU, H. 1981 Deformation of supercritical stable waves on a viscous liquid film down an inclined plane wall with the decrease of wave number. *J. Phys. Soc. Japan* **50**, 1017–1024.

WILLIAMS, M. B. & DAVIS, S. H. 1982 Nonlinear theory of film rupture. *J. Colloid Interface Sci.* **90**, 220–228.

YIANTSIOS, S. G. & HIGGINS, B. G. 1989 Rayleigh–Taylor instability in thin viscous films. *Phys. Fluids* A **1**, 1484–1501.

YIH, C.-S. 1955 Stability of parallel laminar flow with a free surface. *Proc. 2nd US Congr. Appl. Mech.*, pp. 623–628. ASME.

YIH, C.-S. 1963 Stability of liquid flow down an inclined plane. *Phys. Fluids* **6**, 321–334.